Research Square

Preprints are preliminary reports that have not undergone peer review.
They should not be considered conclusive, used to inform clinical practice,
or referenced by the media as validated information.

Differential redox-mitochondrial adaptation to ultra-high dose rate irradiation in astrocytes and glioma cells

Beatrice D'Orsi

beatrice.dorsi@in.cnr.it

Italian National Research Council (CNR) https://orcid.org/0000-0002-4335-3995

Giulia Rosini

Italian National Research Council (CNR)

Elisa De Santis

Italian National Research Council (CNR)

Riccardo Nieri

Italian National Research Council (CNR)

Matteo Paolini

Italian National Research Council (CNR) https://orcid.org/0009-0001-9439-0358

Filippo Rossi

Italian National Research Council (CNR)

Silverio Sbrana

Italian National Research Council (CNR)

Esther Ciarrocchi

University of Pisa

Andrea Cavalieri

University of Pisa

Fabiola Paiar

University of Pisa

Fabio Di Martino

University of PIsa

Eleonora Vannini

Italian National Research Council (CNR)

Mario Costa

Italian National Research Council (CNR)

Article

Keywords: Ultra-High Dose Rate irradiation, FLASH Radiotherapy, redox signaling, mitochondrial dysfunction, bioenergetics, cancer metabolism, glioblastoma

Posted Date: June 8th, 2026

DOI: https://doi.org/10.21203/rs.3.rs-9908162/v1

License: This work is licensed under a Creative Commons Attribution 4.0 International License.
Read Full License

Additional Declarations:
There is no conflict of interest

Tables 1 and 2 are available in the Supplementary Files section.

Differential redox-mitochondrial adaptation to ultra-high dose rate irradiation in astrocytes and glioma cells

Giulia Rosini[1], Elisa De Santis[1,2], Riccardo Nieri[1], Matteo Paolini[1,3], Filippo Rossi[1], Silverio Sbrana[3], Esther Ciarrocchi[4,5,6], Andrea Cavalieri[4,6], Fabiola Paiar[7,8], Fabio Di Martino[5,8,9], Eleonora Vannini[1,6], Mario Costa[1,6] and Beatrice D'Orsi[1,5,6]

[1]Institute of Neuroscience, Italian National Research Council, Pisa, Italy;

[2]Bio@SNS Lab, Scuola Normale Superiore, Pisa, Italy;

[3]Institute of Clinical Physiology, Italian National Research Council, Pisa, Italy;

[4]Department of Physics, University of Pisa, Pisa, Italy;

[5]National Institute of Nuclear Physics, Section of Pisa, Pisa, Italy;

[6]University of Pisa, Center for Instrument Sharing of the University of Pisa (CISUP), Pisa, Italy;

[7]Unit of Radiation Therapy, Department of Translational Research and New Technologies in Medicine and Surgery, University of Pisa, Italy.

[8]Centro Pisano Multidisciplinare Sulla Ricerca e Implementazione Clinica Della Flash Radiotherapy (CPFR), University of Pisa, Italy.

[9]Azienda ospedaliero universitaria pisana, U.O. Fisica Sanitaria, Pisa, Italy.

Beatrice D'Orsi, PhD

beatrice.dorsi@in.cnr.it

Keywords: Ultra-High Dose Rate irradiation, FLASH Radiotherapy, redox signaling, mitochondrial dysfunction, bioenergetics, cancer metabolism, glioblastoma

Abstract

FLASH radiotherapy (FLASH-RT) delivers radiation at ultra-high dose rates (UHDRs) and has been reported to reduce normal tissue toxicity while maintaining tumor control, yet the cellular mechanisms underlying the 'FLASH effect' remain incompletely defined. FLASH/UHDR irradiation has been associated with differential normal and tumor tissue responses in preclinical studies, although the early cellular processes induced under these conditions remain incompletely understood.

Here, we compared FLASH *versus* conventional radiotherapy (CONV-RT) in murine glioma GL261 cells and primary healthy astrocytic cultures, focusing on redox dynamics, mitochondrial function, bioenergetics, and stress transcriptional programs. Using real-time kinetic assays, flow cytometry, Seahorse analysis, and gene expression profiling, we found that in healthy astrocytes FLASH-RT reduced acute ROS accumulation, limited cell death, and promoted relative recovery of mitochondrial membrane potential and respiratory capacity compared to CONV-RT. FLASH irradiation was also associated with sustained induction of cell-cycle checkpoint and senescence-related markers. In GL261 cells, FLASH-RT produced a lower initial ROS peak followed by continued ROS accumulation over time and enhanced G2/M accumulation, together with persistent mitochondrial depolarization and respiratory suppression. Annexin V analysis at 8 Gy revealed comparable levels of apoptosis between FLASH- and CONV-RT, consistent with tumor responses being associated with checkpoint-dependent proliferative constraint and metabolic dysfunction rather than enhanced apoptotic execution. Pharmacological inhibition of PARP, calpains, necroptosis, and caspases differentially modulated mitochondrial bioenergetic parameters across modalities and cell types, supporting pathway-diverse contributions to radiation-induced metabolic stress. Tumor-selective stress responses were also observed in human U87 glioblastoma cells, where FLASH irradiation induced stronger ROS accumulation, enhanced apoptotic engagement, and alterations in NAD^+ levels associated with mitochondrial respiratory impairment compared with CONV-RT. Collectively, these data indicate that FLASH-RT elicits cell-type-specific redox–mitochondrial reprogramming that was associated with relative preservation of mitochondrial function in healthy astrocytes while imposing prolonged metabolic and proliferative constraints in glioma cells, highlighting distinct early redox-mitochondrial adaptations induced by FLASH/UHDR irradiation in astrocytic and glioma models.

Abbreviation

CONV, Conventional; DIC, Differential Interference Contrast; DCF-DA, 2′,7′-Dichlorofluorescein Diacetate; FBS, Fetal Bovine Serum; GL261, murine glioma cell line 261; Gy, gray (unit of absorbed radiation dose); H_2O_2, Hydrogen Peroxide; LC3, Microtubule-Associated Protein 1 Light Chain 3; OCR, Oxygen Consumption Rate; PBS, Phosphate-Buffered Saline; PCR, Polymerase Chain Reaction; PI, Propidium Iodide; qPCR, Quantitative Polymerase Chain Reaction; ROS, Reactive Oxygen Species; RT, Radiotherapy; SEM, Standard Error of the Mean; TMRM, Tetramethylrhodamine Methyl Ester; UHDR, Ultra-High Dose-Rate; U87, Human Glioblastoma Cell Line; $\Delta\psi_m$, Mitochondrial Membrane Potential.

Introduction

FLASH radiotherapy (FLASH-RT) is an emerging cancer treatment modality characterized by the delivery of ultra-high dose rates (UHDRs, > 40 Gy/s) of radiation within milliseconds (1,2), contrasting with conventional radiotherapy (CONV-RT), which administers radiation at lower dose rates (typically < 0.1 Gy/s) over several minutes (3,4). The distinctive feature of FLASH/UHDR irradiation is its potential to spare normal tissues while maintaining or enhancing tumor control, a phenomenon known as the 'FLASH effect' (1,5). However, the cellular and metabolic determinants of this differential response remain actively debated. Among the proposed mechanisms underlying the FLASH effect, redox balance and mitochondrial metabolism have emerged as central candidates. Ionizing radiation induces reactive oxygen species (ROS), which contribute to DNA damage and cell death but also regulate stress signaling and adaptive responses (6–9). While the FLASH effect is ultimately defined by differential normal tissue sparing *in vivo*, *in vitro* systems remain valuable for investigating early cell-intrinsic responses induced by FLASH/UHDR irradiation. Compared with CONV-RT, FLASH-RT has been proposed to alter radiochemical and cellular redox kinetics, potentially reducing the persistence of damaging oxidative species in normal tissues while differentially modulating oxidative stress responses in tumor cells (10,11). While early models emphasized transient oxygen depletion as a primary driver of the FLASH effect, increasing evidence suggests that mitochondrial metabolism and redox adaptation may play critical complementary roles. Because mitochondria are both a major source and a primary target of ROS, mitochondrial membrane potential ($\Delta\Psi_m$), respiratory activity, and redox buffering capacity have emerged as key determinants of differential cellular adaptation under FLASH irradiation conditions (8,12,13). Differences in mitochondrial adaptability and antioxidant capacity between normal and tumor cells may therefore critically influence radiation sensitivity under these irradiation conditions.

Cancer cells exhibit metabolic rewiring that supports proliferation and therapy resistance, including altered redox buffering and flexible engagement of oxidative phosphorylation (OXPHOS) and glycolysis depending on energetic demands and stress conditions (14–17). This metabolic plasticity may influence radiation sensitivity: mitochondrial failure can amplify ROS and trigger cell death pathways, whereas mitochondrial resilience can contribute to recovery from oxidative stress and maintenance of proliferative capacity.

Glioblastoma (GBM) remains among the most aggressive and treatment-resistant primary brain tumors. Despite surgery, chemotherapy, and radiotherapy, median survival remains limited, reflecting profound radioresistance, metabolic adaptability, and intratumoral heterogeneity (18–22). Understanding whether FLASH/UHDR irradiation induces distinct redox-mitochondrial responses in glioma *versus* healthy brain cells could inform strategies to widen the therapeutic window in GBM-relevant settings.

In this study, we compared GL261 glioma cells and primary healthy astrocyte cultures exposed to FLASH *versus* CONV irradiation. GL261 is a widely used syngeneic murine glioma model that allows investigation of tumor-immune interactions in immunocompetent hosts, although it displays higher immunogenicity and distinct genomic and metabolic features compared with human glioblastoma (23). By integrating real-time ROS kinetics, mitochondrial flow cytometry readouts, Seahorse-based bioenergetic profiling, and stress transcriptional analysis, we sought to determine whether FLASH-RT differentially modulates mitochondrial function and post-irradiation bioenergetic adaptation in tumor *versus* normal brain cells. To further probe the contribution of regulated cell death signaling to radiation-induced metabolic collapse, we employed pharmacological inhibitors targeting PARP, calpains, necroptosis, and caspases as functional probes. Together, this approach enables the interrogation of cell-type-specific redox and metabolic responses engaged by the two irradiation modalities, with particular focus on how mitochondrial dysfunction may constrain post-irradiation proliferative recovery in glioma cells. Because glioblastoma displays marked metabolic heterogeneity across experimental models and patients, we further extended our analysis to human U87 glioblastoma cells (24,25). We aimed to determine whether FLASH-induced redox-mitochondrial responses are conserved across tumor systems with distinct metabolic wiring. These insights are essential for the rational optimization of dose-rate paradigms and may inform strategies aimed at expanding the therapeutic window of radiotherapy in GBM-relevant experimental systems.

Materials and Methods

Materials

Unless otherwise stated, all chemicals, including DMEM/F12 medium, fetal bovine serum (FBS), phosphate-buffered saline (PBS), trypsin, carbonyl cyanide 4-(trifluoromethoxy) phenylhydrazone (FCCP), tert-butyl hydroperoxide (TBHP), Calpeptin, carbobenzoxy-valyl-alanyl-aspartyl-[O-methyl]-fluoromethylketone (z-VAD-FMK), 3,4-dihydro-5-[4-(1-piperidinyl) butoxy]-1(2H)-isoquinoline (DPQ), and Necrostatin-1 (Nec-1), were purchased from Sigma-Aldrich. MitoTracker™ Green, MitoTracker™ Red CMXRos, CellROX™, tetramethylrhodamine methyl ester (TMRM) and Annexin V were obtained from Thermo Fisher Scientific. Reagents for Seahorse assays were obtained from Agilent Technologies, including XF DMEM medium (pH 7.4), XF 1 M glucose solution, XF 100 mM pyruvate solution, XF 200 mM glutamine solution, and lyophilized compounds for the Mito Stress Test (Oligomycin, FCCP, and the Rotenone/Antimycin A mix).

Linear accelerator (LINAC)

We used the ElectronFlash (EF) linear accelerator (26), installed in a dedicated bunker at the Centro Pisano FLASH Radiotherapy (CPFR, Pisa, Italy). This electron accelerator (7 and 9 MeV) allows for variation of the pulse repetition frequency (PRF, 1–245 Hz) and pulse duration (0.1 - 4 μs), as well as, thanks to the triode gun, the beam current (1 - 100 mA). This allows independent modification of both the average-dose-rate (ADR) and the dose-per-pulse (DPP), without changing the energy spectrum or the experimental setup, in a range from that typical of CONV treatments to very high FLASH/UHDR conditions. Dose distribution uniformity is achieved using mechanical PMMA collimators (applicators) of cylindrical shape and varying lengths and dimensions. EF is equipped with an accurate and non-invasive monitoring system based on an ACCT system (https://www.bergoz.com/products/acct). The dosimetric characterization of the beams produced by EF was performed using the flashDiamond (fD) detector (27) and other dosimeters and techniques, including those developed internally at CPFR (28–31) and provided by other research groups (32–35).

***In vitro* irradiations**

For the *in vitro* irradiations, EF was operated at 9 MeV and the largest available PMMA applicator (∅120 mm; Fig. S1), ensuring a dose distribution homogeneity within 95% across the entire area of the petri dishes. A 12 mm-thick PTW solid water slab was placed at the end of the applicator to reach the build-up region of uniform dose for the 9 MeV beam (Fig. S1). This configuration ensures uniform and reproducible irradiation conditions *in vitro*. Table 1 summarizes the main dosimetric parameters used for CONV and FLASH irradiations. The delivered doses were 4, 8, and 16 Gy, and the ADR was kept constant at 240 Gy/s, a value that exceeds the threshold required to trigger the FLASH effect (100 Gy/s). This was achieved by adjusting the PRF, since the ADR, neglecting the pulse width, can be defined as:

$$ADR = \frac{n}{n-1} \cdot DPP \cdot PRF$$

Cell lines

The mouse glioma GL261 cells (36,37) and human glioblastoma cells U87 (38,39) were maintained in DMEM/F12 (1:1) medium containing 10 % FBS, 100 μg/mL penicillin-streptomycin, and 2 mM L-glutamine. Cells were maintained at 37 °C in a humidified incubator with 5% CO_2.

Primary healthy astrocytic cell preparation

Mouse primary cortical astrocyte isolation was performed using cortices of postnatal day 0-2 (P0-P2) C57BL/6 wild-type pups (40,41). After the dissection, DMEM/F12 (1:1) medium supplemented with 10 % FBS, 100 µg/mL penicillin-streptomycin was added to the tissues. Tissue was then dissociated by gentle pipetting, sifted through a 70-µm cell strainer (Sarstedt) using a syringe plunger and centrifuged at 300 x g for 15 min at room temperature (RT). The pellet was washed twice with 25 mL of supplemented medium. Cells were seeded at a density of 5×10^6 cells/10 mL in cell culture T75 flasks and incubated at 37 °C, 5% CO_2. Cells were split every 5 - 7 days and used for ≤ 3 passages. All procedures were approved by the institutional animal ethics committee, and tissues were obtained from animals not used in other experiments.

Time-lapse cellular ROS measurements

GL261 and astrocytic cells were seeded at 5,000 cells/well in 96-well plates (n = 6), allowed to adhere overnight, and for 40 min at 37 °C with 20 µM DCFDA/H_2DCFDA (Cellular ROS Assay Kit, Abcam) in Krebs buffer (KB; 140 mM NaCl, 5.9 mM KCl, 1.2 mM $MgCl_2$, 15 mM HEPES, pH 7.4) supplemented with 10 mM D-glucose and 2.5 mM $CaCl_2$. DCFDA is deacetylated by intracellular esterases into non-fluorescent DCFH, which is oxidized by ROS into fluorescent DCF. After incubation, probe solution was replaced with fresh KB, and a 5-min baseline fluorescence was recorded (Varioskan™ LUX, 485/535 nm). Cells were irradiated (FLASH or CONV) and monitored for 2 h. Untreated cells were controls; H_2O_2 was positive control. At 125 min, 200 µM TBHP induced a maximal ROS burst. Irradiated medium-only controls were included, quantified, and evaluated during the initial Ca^{2+} and ROS kinetic experiments and considered negligible in the context of the overall cellular ROS responses.

Transcriptional gene activation using RT-qPCR

GL261 and astrocytic cells were seeded at 60,000 and 80,000 cells/well in 6-well plates (3 wells per condition) and exposed to 8 Gy (FLASH or CONV) or left untreated. RNA was extracted at 0, 1, 6, 24, and 72 h post-irradiation using RNeasy Mini Kit (Qiagen). cDNA was synthesized from 1 µg RNA (Reverse Transcriptase Core Kit, Eurogentec). qPCR was performed with PowerUp SYBR™ Green Master Mix (Applied Biosystems) using β-actin as internal control. Relative expression was calculated via 2^−ΔΔCt. Primer sequences: 5'-CCATGGCCATCTACAAGAAG-3' and 5'-TTTCCTTCCACCCGGATAAG-3' for *p53*; 5'-AGCAAAGTGTGCCGTTGTC-3' and 5'-TCTCCGTGACGAAGT CAAAG-3' for *p21*; 5'-AACTGCAGGAGAGCCATCTG-3' and 5'-GGGTACGACCGAAAGAGTTC-3' for *p16*; 5'-GGCCTCCTCTCCTACTTCGG-3' and 5'-TGAGGACTCCAGCCACAAAGA-3' for *Bax*; 5'-TGTGTGTGGAGAGCG

TCAACA-3' and 5'-TGCCGGTTCAGGTACTCAGTC-3' for *Bcl2*; 5'-CTGCCTGTCCTGGATAAGACCA-3' and 5'-CTGGTTGACCAGCAGGAAGAAG-3' for *Lc3*; 5'-CAGCCTCTGAAACTGGACACGA-3' and 5'-CTCTCC TGAGTTAGCCTCTTCC-3' for *Beclin1*; 5'-CTCTGTGTGGATCGGTGGCT-3' and 5'-CTGCTTGCTGATCCACATCTG-3' for *β-actin*.

Flow cytometry

Annexin V apoptosis assay

GL261 and U87 cells were seeded at 40000 and 30000 cells/well, respectively, in 24-well plates and irradiated (8 Gy, FLASH or CONV). At 72 h post-irradiation, cells were harvested, washed in cold PBS, and resuspended in Annexin V binding buffer. Cells were then stained with Annexin V according to the manufacturer's instructions (ThermoFisher Scientific) and incubated for 15 min at RT in the dark. Following incubation, samples were diluted with 400 µl of Annexin V binding buffer and immediately analyzed by flow cytometry (CytoFLEX V2-B2-R2, Beckman Coulter). Apoptotic cells were identified based on Annexin V positivity and results were expressed as the percentage of Annexin V-fluorescence.

Cell cycle analysis by Propidium Iodide staining

GL261 cells were seeded at 100000 cells/well in 6-well plates and irradiated (8 Gy, FLASH or CONV). At 24 and 72 h post-irradiation, cells were harvested, washed twice with PBS, and fixed in 95% cold ethanol at RT for 5 minutes. Following fixation, cells were washed with PBS and incubated with 50 µg/ml Propidium Iodide (PI) staining solution (Biolegend) containing RNase A for 30 min at RT in the dark. Samples were then analyzed by flow cytometry (CytoFLEX V2-B2-R2, Beckman Coulter). Cell cycle distribution was determined based on DNA content and expressed as the percentage of PI fluorescence in G0/G1, S, and G2/M phases.

Mitochondrial dynamics and bioenergetics

Cells were seeded at 60.000 (astrocytes) and 40.000 (GL261) cells/well in 24-well plates and irradiated (8 Gy, FLASH or CONV). At 0, 1, 6, 24, and 72 h, cells were incubated with 50 nM MitoTracker Green, MitoTracker Red CMXRos, TMRM, or CellROX Green for 30 min at 37 °C in the dark. Cells were washed 3× with PBS, centrifuged at 1000 RPM for 5 min, and analyzed by flow cytometry (≥ 40.000 events/sample, CytoFLEX V2-B2-R2, Beckman Coulter). Fluorescence was expressed as mean fluorescence intensity.

Metabolic profile analysis

GL261 and astrocytic cells were seeded in XF96-well plates at 8×10^4 cells/well and incubated 24 h. Cells were irradiated (8 Gy, FLASH or CONV) or left untreated. Cells were equilibrated in XF DMEM medium (pH 7.4) for 45 - 60 min at 37 °C in a non-CO_2 incubator. Mito Stress Test reagents (Oligomycin 3 µM, FCCP 1 µM, Antimycin A/Rotenone 1 µM each) were sequentially injected using a Seahorse XF Pro Analyzer (Agilent Technologies) (42). OCR was normalized to total protein content (µg, Pierce BCA kit) to quantify basal respiration, ATP-linked respiration, proton leak, maximal respiration, spare respiratory capacity, and non-mitochondrial respiration. Cells were pre-treated 16 h with DPQ (100 µM), z-VAD-FMK (100 µM), Necrostatin-1 (50 µM), or Calpeptin (20 µM) to dissect contributions of specific cell death pathways.

Cellular ATP quantification

Cellular ATP was quantified using CellTiter-Glo® luminescence assay (Promega). Cells were seeded at a density of 4,000 cells per well in an opaque 96-well plate (ThermoFisher) and allowed to adhere overnight in the incubator. Three control wells containing only culture medium (no cells) were included to determine background luminescence. ATP levels were quantified according to the manufacturer's instructions. Briefly, 100 µL of assay buffer was added to each well containing 100 µL of culture medium, and the plate was incubated for 2 minutes at RT on a shaker. The plate was then left at RT for an additional 10 minutes to stabilize the luminescence signal, after which luminescence was measured using a Varioskan™ LUX (Thermo Fisher Scientific) with a settling time of 1000 ms. Protein concentration was assessed with BCA kit (Pierce) in order to account for differences in cell number. Serial fold dilutions of ATP were prepared to generate an ATP standard curve and µM of ATP normalized to protein concentration.

Cellular NAD^+/NADH quantification

Cellular NAD^+/NADH was quantified using NAD^+/NADH-Glo® luminescence assay (Promega). Cells were seeded at a density of 50,000 cells per well in an optical-bottom 96-well plate (ThermoFisher) and allowed to adhere overnight in the incubator. Three control wells containing only culture medium (no cells) were included to determine background luminescence. NAD^+/NADH levels were quantified according to the manufacturer's instructions. Briefly, 50 µL of detection reagent was added to each well containing 50 µL of culture medium, and the plate was briefly shaken to ensure proper mixing. The plate was then incubated at RT for 30 minutes to allow stabilization of the luminescence signal. Luminescence was subsequently measured using a Varioskan™ LUX (Thermo Fisher Scientific) with a settling time of 1000 ms. Protein concentration was determined using the BCA kit (Pierce) in order to account for differences in cell number. Serial dilutions

of NAD^+ standards were prepared to generate an NAD^+ standard curve, and NAD^+ levels were expressed as nM of NAD^+ normalized to protein concentration.

Statistical analysis

Experiments were performed at least three independent experiments. Data are presented as mean ± SEM. Analyses were performed using GraphPad Prism 10, with one- or two-way ANOVA followed by Tukey's post hoc test. $p < 0.05$ was considered significant; exact p-values are reported in figure legends.

Results

FLASH-RT reduces oxidative stress and cell death in healthy astrocytes while preserving checkpoint and senescence pathways

To evaluate the oxidative and molecular responses induced by FLASH-RT and CONV-RT, we performed a multiparametric analysis of ROS dynamics, Ca^{2+} signaling, cell death, and transcriptional responses in healthy primary murine astrocytes exposed to 8 Gy irradiation. We also refer to our previously published data in ARPE-19 cells, where FLASH-RT preferentially spared non-transformed cells *in vitro* and *in vivo*. The 8 Gy dose was selected because it revealed the most robust FLASH-sparing effect in our experimental models (43). Non-irradiated cells served as controls. Notably, all irradiations were performed using the EF linear accelerator installed at the CPFR (Pisa, Italy; see Materials and Methods section), using a highly reproducible irradiation platform enabling both FLASH and CONV conditions. Time-lapse calcium imaging using Fluo4-AM showed that both modalities similarly increased intracellular Ca^{2+} over time (Fig. S2a, b). Importantly, time-lapse ROS measurements using DCFDA revealed that both irradiation modalities triggered rapid ROS accumulation detectable within minutes after irradiation. However, ROS levels were significantly lower in FLASH-RT-treated cells, indicating reduced acute oxidative stress (Fig. 1a - c). Additional analysis of ROS levels between 30 min post-irradiation and the end of the experiment, including the rate of fluorescence increase (Slope), did not reveal any further significant differences between conditions (data not shown), indicating recovery of redox homeostasis after the early post-irradiation phase. Compatible with reduced oxidative stress, cell death at 72 h was significantly lower in FLASH-RT (~ 35%) than in CONV-RT (~ 65%), although both were elevated compared to controls (Fig. 1d, e). To investigate transcriptional responses underlying these effects, mRNA levels of *p53*, *p21*, and *p16* were quantified over 72 h (Fig. 1f). *p53* expression showed a modest early decrease followed by a gradual increase in both modalities compared to controls; however, this did not reach statistical significance (Fig. 1f, left panel). *p21*, a key effector of p53-mediated cell cycle arrest,

was rapidly and robustly induced by FLASH-RT, peaking at 6 h and remaining elevated, whereas CONV-RT triggered only a moderate increase (Fig. 1f, middle panel). *p16*, a senescence-associated marker, exhibited minimal early changes following FLASH-RT, although trends may suggest activation of a senescence-like program at later time points (Fig. 1f, right panel). Additional stress- and DNA-damage-related targets showed no significant modulation (data not shown). These results indicate that FLASH-RT is associated with reduced ROS levels and lower cell death in healthy astrocytes, together with modulation of *p21* and *p16* expression, supporting differential early redox and stress-adaptive responses under FLASH irradiation conditions.

FLASH-RT induces sustained ROS accumulation and stress-associated transcriptional responses with G2/M checkpoint engagement in GL261 cells

Having established that FLASH-RT preserves redox balance in healthy astrocytes, we next examined tumor cell responses using GL261 glioma cells. ROS dynamics were monitored in real time using DCFDA. At 8 Gy, both FLASH- and CONV-RT induced an immediate increase in ROS levels, with FLASH-treated cells displaying a lower initial peak (Fig. 2a - c). In contrast to healthy astrocytes (Fig. 1b, c), this early reduction was followed by prolonged ROS accumulation over time in FLASH-treated GL261 cells (Fig. 2a - c). Radiation-induced apoptosis was assessed at 72 h by Annexin V staining following 8 Gy irradiation. Both FLASH- and CONV-RT induced comparable increases in Annexin V-positive cells compared to control, indicating comparable apoptotic engagement between the two irradiation modalities (Fig. 2d). Consistently, clonogenic survival assays performed at 4, 6, and 8 Gy showed a dose-dependent reduction in colony formation, with a marked decrease in survival at 8 Gy under both irradiation modalities (Fig. S2c, d). Moreover, dose-dependent increases in cell death at 72 h were observed across 4, 8, and 16 Gy for both irradiation modalities (Fig. S2e), accompanied by a corresponding reduction in cell density (Fig. S2f). At 72 h, cell death differed in a dose-dependent manner: higher after FLASH at 4 Gy, similar at 8 Gy, and lower after FLASH at 16 Gy. Confocal imaging further revealed nuclear enlargement (2 - 3-fold larger than normal) following irradiation under both modalities (Fig. S2g, h), with increased nuclear size observed under FLASH-RT at 4 Gy, suggesting enhanced nuclear swelling following FLASH irradiation at lower doses. However, the proportion of enlarged nuclei remained comparable across doses (data not shown). Time-lapse calcium imaging using Fluo4-AM revealed increased intracellular Ca^{2+} levels following both irradiation modalities. CONV-RT induced higher Ca^{2+} fluxes at the time of irradiation, whereas FLASH-RT elicited stronger Ca^{2+} elevations at later time points (data not shown; two-way ANOVA followed by Tukey's post hoc test: Ca^{2+} Peak $p = 0.0003$ CONV *vs* Control 4 Gy; $p = 0.0161$ CONV *vs* Control 8 Gy; $p = 0.0136$ FLASH *vs* CONV 4 Gy; Ca^{2+} Slope $p = 0.043$ FLASH *vs* CONV 4

Gy). Subsequently, gene expression analysis highlighted modality-specific transcriptional responses (Fig. 2e - g). *Bax*, a pro-apoptotic gene, was strongly upregulated after both irradiation modalities, with earlier and higher induction under FLASH, whereas *Bcl-2*, an anti-apoptotic gene, showed transient upregulation followed by decline in FLASH-treated cells, suggesting stronger early pro-apoptotic transcriptional priming under FLASH (Fig. 2e). *p53*, *p21*, and *p16* were induced earlier and more robustly by FLASH-RT, particularly at 24 - 72 h, consistent with activation of stress and checkpoint responses, including senescence-associated transcriptional changes (Fig. 2f). Autophagy-related genes (*Lc3*, *Beclin1*) were also more rapidly and strongly induced by FLASH-RT, peaking between 24 and 72 h (Fig. 2g). Reliably, PI-based cell cycle analysis showed a reduction in G0/G1 and S phase fractions with a concomitant accumulation of GL261 cells in G2/M at 24 h post-irradiation under both FLASH and CONV conditions (Fig. 2h, i). Notably, FLASH-treated cells exhibited a higher proportion of cells in G2/M compared to CONV at 24 h, with a persistent trend at 72 h, possibly indicating enhanced checkpoint engagement following FLASH irradiation.

FLASH-RT maintains mitochondrial integrity in healthy astrocytes but promotes dysfunction in GL261 cells

To further characterize mitochondrial function and oxidative stress following irradiation, we assessed, at 8 Gy, mitochondrial parameters over the 72 h post-irradiation period in healthy astrocytes and GL261 cells using flow cytometry (Fig. 3, Fig. S3a). In healthy astrocytes, MitoTracker Green, MitoTracker Red CMXRos, and TMRM revealed that mitochondrial mass, $\Delta\Psi_m$, and respiratory activity recovered more robustly after FLASH-RT compared to CONV-RT (Fig. 3a - c, i, Fig. S3), indicating improved mitochondrial homeostasis. CellROX measurements confirmed lower ROS accumulation under FLASH-RT (Fig. 3d, i). In GL261 cells, early mitochondrial responses were comparable between irradiation modalities, with transient increases in mitochondrial mass and membrane potential. At later time points (24 - 72 h), FLASH-RT caused greater $\Delta\Psi_m$ loss and continued ROS accumulation (Fig. 3e - h, j, Fig. S3b). Differences between FLASH and CONV irradiation partially converged over time in healthy astrocytes, whereas chronic mitochondrial alterations were observed in GL261 tumor cells (Fig. 3i - j).

FLASH-RT preserves bioenergetic function in astrocytes but suppresses mitochondrial respiration in GL261 cells

Having observed the engagement of multiple stress and cell-death-related pathways in parallel, we next profiled, at 8 Gy, mitochondrial respiration in healthy astrocytes and GL261 cells using the Seahorse XF Cell Mito Stress Test (Fig. 4, 5). To characterize bioenergetic responses and explore pathway-specific contributions to FLASH- and CONV-RT, prior to irradiation, cells were pre-treated with inhibitors targeting PARP (DPQ), calpains (Calpeptin), necroptosis (Nec-1), and

caspases (zVAD). In healthy astrocytes, basal and maximal respiration were partially suppressed by both modalities, whereas FLASH-RT maintained higher spare respiratory capacity and lower proton leak compared to CONV-RT (Fig. 4a, f), indicating preserved bioenergetic flexibility. Differences in respiratory parameters partially converged at later time points. Inhibitor treatments differentially affected mitochondrial respiration across irradiation modalities. CONV-RT-induced mitochondrial impairment appeared to involve PARP activation, necroptosis, and calpain activity, whereas apoptotic signaling played a more limited role. In contrast, inhibitor treatments produced limited rescue of respiration after FLASH compared with CONV (Fig. 4b - f). In GL261 cells, FLASH-RT induced stronger and more persistent suppression of basal, ATP-linked, and maximal respiration compared to CONV-RT (Fig. 5a, f). DPQ treatment predominantly restored respiratory parameters under CONV conditions (Fig. 5b, f). zVAD partially restored respiration under both conditions, with a pronounced increase in NMR after FLASH (Fig. 5c, f). Nec-1 and Calpeptin selectively enhanced BR and ATP-linked respiration under FLASH-RT (Fig. 5d, e, f). Notably, inhibitor treatments also reduced proton leak under both irradiation modalities. Collectively, these results demonstrate that FLASH-RT differentially modulates mitochondrial and oxidative responses in healthy astrocytes and GL261 cells.

FLASH-RT promotes mitochondrial oxidative stress and bioenergetic imbalance in human U87 glioblastoma cells

To explore whether the redox-mitochondrial responses observed in murine GL261 glioma cells were conserved across additional tumor models, we extended our analysis to human U87 glioblastoma cells (Fig. 6). Annexin V staining revealed a marked increase in apoptotic cells following FLASH-RT compared with both control and CONV-RT conditions, indicating stronger apoptotic engagement under FLASH irradiation than conventional irradiation (Fig. 6a). Analysis of $\Delta\Psi_m$ showed a transient increase at early time points followed by a progressive decline at later stages after both irradiation modalities (Fig. 6b), suggesting an initial phase of mitochondrial hyperactivation preceding mitochondrial dysfunction. In parallel, intracellular ROS levels increased markedly after irradiation, with FLASH-treated U87 cells exhibited significantly higher ROS accumulation compared with CONV-RT at 24 h (Fig. 6c). In line with these oxidative changes, metabolic analyses revealed alterations in cellular bioenergetic status. Intracellular ATP levels progressively declined following both FLASH and CONV irradiation (Fig. 6d). In contrast, NAD^+ levels increased significantly at later time points, with a more pronounced accumulation in FLASH-treated cells compared with CONV-RT, suggesting activation of metabolic stress responses associated with oxidative damage and redox imbalance (Fig. 6e). Seahorse bioenergetic profiling further demonstrated impaired mitochondrial respiration following irradiation, characterized by reduced basal respiration, ATP-linked respiration, maximal respiration, and spare respiratory capacity under both irradiation modalities (Fig. 6f). Together,

these findings indicate that in U87 glioblastoma cells FLASH-RT may induce stronger oxidative stress, greater NAD^+ accumulation, and enhanced apoptotic engagement compared with CONV-RT, consistent with FLASH-induced mitochondrial oxidative stress and bioenergetic imbalance in this tumor model.

Discussion

This study provides an integrated multiparametric analysis combining redox, mitochondrial, transcriptional, and regulated cell-death profiling to delineate the differential cellular responses to FLASH/UHDR *versus* CONV irradiation in healthy astrocytes and glioma cells. Our data reveal a coherent redox–mitochondrial response program that distinguishes normal astrocytes from glioma cells following irradiation (summarized in Table 2). In healthy astrocytes, FLASH reduced oxidative stress, preserved mitochondrial integrity and bioenergetic flexibility, limited cell death, and was associated with sustained activation of cell cycle checkpoint and senescence-related pathways. In contrast, in GL261 glioma cells, FLASH-RT induced sustained ROS accumulation, prolonged checkpoint engagement, and persistent mitochondrial dysfunction, despite comparable levels of early apoptotic commitment relative to CONV-RT, indicating that differential tumor responses to FLASH are unlikely to be driven by enhanced apoptotic susceptibility *per se*. Collectively, our results suggest that FLASH/UHDR irradiation was associated with differential redox, mitochondrial, and proliferative responses between healthy astrocytes and glioma cells, consistent with emerging evidence from *in vitro* and *in vivo* models (1,44,45). Importantly, these biological responses do not imply the existence of a single unifying mechanism underlying the FLASH effect. Rather, our findings suggest that redox-mitochondrial regulation represents one important cellular layer contributing to the differential response between normal and tumor cells. In fact, these observations should be interpreted as context-dependent and model-dependent, reflecting the specific cellular systems, metabolic states, and experimental conditions under which FLASH/UHDR irradiation is delivered. Recent literature has proposed that redox-mitochondrial regulation may contribute to differential biological responses observed under FLASH irradiation conditions (46).

In normal astrocytes, FLASH-RT induced a smaller acute ROS burst compared to CONV-RT and markedly lower cell death at 72 h (Fig. 1). This differential ROS profile is in agreement with the oxygen depletion/reduced peroxyl radical yield hypothesis, whereby FLASH irradiation transiently limits oxygen availability and reduces the propagation of long-lived oxidative radicals (47). Although our experiments primarily capture astrocyte-driven responses, emerging evidence indicates that myeloid lineage cells may exhibit distinct ROS regulatory programs under FLASH irradiation (48), raising the possibility that cell-type-specific redox regulation across neural and immune compartments contributes to the integrated tissue-level responses associated with the FLASH effect *in vivo*. FLASH-RT also preserved $\Delta\Psi_m$ and mitochondrial activity

more effectively than CONV-RT, indicating improved maintenance of mitochondrial homeostasis (Fig. 3). Despite lower oxidative and metabolic stress, FLASH-treated astrocytes exhibited continued *p21* induction and late *p16* expression, suggesting activation of checkpoint-mediated growth arrest rather than engagement of apoptotic cell death pathways (Fig. 1). This pattern is in line with the maintenance of proliferative arrest without loss of viability and mirrors observations in normal lung and intestinal tissues exposed to FLASH irradiation, where clonogenic survival and tissue function are preserved (24,49–51). Minor baseline fluctuations in some transcripts likely reflect technical variability or transient handling effects and do not affect interpretation. Mechanistically, lower cumulative oxidative burden may arise from transient oxygen depletion during FLASH delivery, reducing radiochemical oxygen fixation (52). Furthermore, the radiation-induced bystander effect, intercellular communication mediated by ROS, cytokines, and calcium signaling, (45,53–55). This preservation of normal astrocytic viability is especially relevant in the context of GBM therapy, where radiation-induced cognitive toxicity remains a major clinical limitation (56). In GL261 glioma cells, FLASH-RT produced a lower initial ROS peak but a sustained ROS accumulation over time, in contrast to the transient ROS dynamics observed in astrocytes, indicating a fundamental divergence in redox adaptation between normal and tumor cells (Fig. 2). Although Annexin V analysis revealed comparable levels of apoptotic engagement between FLASH and CONV irradiation at 8 Gy, FLASH-treated GL261 cells displayed increased accumulation in G2/M phase at 24 h, with a persistent trend at 72 h. This dissociation between early apoptotic commitment and cell-cycle redistribution suggests that FLASH-RT may preferentially impair proliferative recovery through checkpoint-mediated growth arrest rather than through increased apoptotic execution. In line with this interpretation, earlier transcriptional activation of stress-associated targets, including *Bax*, *p21*, and *p16*, together with induction of autophagy-related genes, such as *Lc3* and *Beclin1* (Fig. 2), supports engagement of coordinated stress-adaptive programs downstream of sustained oxidative burden, which may be associated with cell cycle arrest and reduced proliferative competence despite comparable early apoptotic responses. Notably, tumor cells often display reduced metabolic flexibility compared with normal cells, making them particularly vulnerable to sustained mitochondrial stress and redox imbalance.

Mitochondrial functional analyses further revealed modality-specific effects. In healthy astrocytes, FLASH-RT supported recovery of mitochondrial activity following irradiation, whereas in GL261 cells it was associated with loss of $\Delta\Psi_m$ and persistent ROS accumulation at later time points (Fig. 3). These observations suggest that although early apoptotic responses are comparable between irradiation modalities, FLASH-RT may impose a prolonged metabolic constraint on tumor cells through mitochondrial failure and redox imbalance, thereby limiting proliferative recovery independently of early apoptotic commitment. These findings are consistent with reports describing differential mitochondrial responses

404 under FLASH irradiation conditions in normal fibroblasts and intestinal crypts (57,58). Bioenergetic profiling using the
405 Seahorse XF Cell Mito Stress Test confirmed these divergent responses. In healthy astrocytes, FLASH-RT preserved spare
406 respiratory capacity and reduced proton leak relative to CONV-RT, corresponding to maintenance of bioenergetic
407 flexibility (Fig. 4). In GL261 cells, FLASH-RT induced stronger and more persistent suppression of basal, ATP-linked,
408 and maximal respiration (Fig. 5). Differential responses to PARP, necroptosis, and calpain inhibition suggest that
409 mitochondrial impairment under CONV-RT may involve PARP-dependent metabolic crisis and calcium-dependent
410 proteolysis. These pathways may contribute to the metabolic instability observed following conventional irradiation (59).
411 In contrast, FLASH-RT was associated with a bioenergetic phenotype consistent with sublethal metabolic stress in healthy
412 astrocytes but sustained respiratory suppression in tumor cells. Importantly, these bioenergetic differences persisted
413 functionally even when basal respiratory parameters partially normalized at later time points, raising the possibility that
414 early mitochondrial responses may shape divergent long-term proliferative outcomes in normal *versus* tumor cells. These
415 observations are compatible with the G2/M accumulation observed in FLASH-treated GL261 cells and support a model in
416 which persistent mitochondrial dysfunction contributes to checkpoint-dependent proliferative arrest rather than immediate
417 apoptotic commitment. Because inhibitor treatments may also act on upstream metabolic checkpoints, their effects likely
418 reflect both direct and indirect modulation of radiation-induced stress pathways and should therefore be interpreted as
419 functional indications rather than definitive evidence of pathway activation. In fact, inhibitors were used here as functional
420 probes of pathway contribution rather than as definitive markers of pathway activation. This strategy enabled the
421 identification of regulated cell death mechanisms potentially contributing to radiation-induced mitochondrial and metabolic
422 dysfunction in healthy *versus* tumor cells. Taken together, our data support a model in which FLASH-RT reduces acute
423 oxidative stress in normal astrocytes while inducing sustained redox imbalance, mitochondrial malfunction, and
424 checkpoint-mediated growth arrest in tumor cells (60–64). In this framework differential tumor cell responses under
425 FLASH/UHDR irradiation may arise from differential redox resilience and mitochondrial adaptability (65,66), rather than
426 from enhanced apoptotic susceptibility *per se*. However, the balance between protection of normal cells and metabolic
427 vulnerability of tumor cells is likely to be strongly context-dependent, influenced by factors such as tissue oxygenation,
428 intrinsic metabolic wiring, and the specific tumor model examined. These findings are also in agreement with recent
429 literature indicating that FLASH irradiation may differentially influence regulated cell death signaling compared with
430 conventional dose rates, reducing apoptotic execution in normal tissues while enhancing stress-adaptive or immunogenic
431 death in tumors (67–71). The distinct inhibitor profiles observed here suggest that therapeutic co-targeting of specific death
432 pathways, for instance, combining calpain or necroptosis modulators with FLASH, may potentiate tumor control without

compromising normal tissue protection (72). This mechanistic diversity may be particularly useful for GBM, where intratumoral heterogeneity often limits the efficacy of single-mode cytotoxic treatments. Moreover, these results highlight the distinct mitochondrial and metabolic responses associated with different irradiation dose-rate modalities in shaping mitochondrial and bioenergetic outcomes, consistent with the growing literature on FLASH-induced modulation of oxidative metabolism (11,69,71). Given that GBM cells are known to rely heavily on redox buffering and mitochondrial rewiring to survive radiotherapy (73), persistent redox-mitochondrial stress induced under FLASH/UHDR conditions may contribute to limiting proliferative recovery in GBM models by limiting proliferative recovery through constant metabolic stress. Although GL261 represents a simplified murine model and does not recapitulate the full molecular and metabolic heterogeneity of human GBM, it has been shown that GL261 tumors exhibit higher immunogenicity and a distinct immune microenvironment compared with human glioblastoma (23,74). To further examine whether tumor responses to FLASH irradiation are conserved across glioma models, we extended our analysis to human U87 glioblastoma cells (75). While GL261 cells predominantly exhibited checkpoint-mediated proliferative arrest associated with mitochondrial dysfunction (Fig. 2 and 5), U87 cells displayed a stronger apoptotic response accompanied by elevated ROS levels and bioenergetic imbalance (Fig. 6). These differences likely reflect intrinsic metabolic heterogeneity among glioma cells, which differ in mitochondrial dependency, redox buffering capacity, and metabolic plasticity (76,77). Such metabolic diversity may determine whether tumor cells respond to FLASH-induced oxidative stress by entering checkpoint-mediated proliferative arrest or by undergoing mitochondrial collapse followed by apoptotic engagement. Tumor cells with reduced redox buffering capacity or lower mitochondrial adaptability may be less able to tolerate sustained oxidative stress induced by FLASH irradiation. These findings further support the notion that cellular responses to FLASH irradiation are strongly context- and model-dependent. The observed increase in NAD^+ levels in U87 cells may reflect activation of PARP-dependent DNA damage responses and compensatory metabolic rewiring aimed at sustaining redox homeostasis during oxidative stress (78). Importantly, these results should be interpreted within the setting of a reductionist *in vitro* model and do not aim to capture the full biological heterogeneity of patient-derived GBM. Accordingly, the mechanisms identified here should be considered model-dependent and will require validation across additional tumor and *in vivo* models.

From a translational perspective, the ability of FLASH/UHDR irradiation to preserve mitochondrial and bioenergetic homeostasis in healthy astrocytes while promoting sustained oxidative and metabolic stress in glioma cells suggests a differential biological response that may be relevant for GBM, where radiation-induced neurotoxicity limits dose escalation. To enable rigorous mechanistic comparison between FLASH and CONV conditions, the present study was intentionally performed using a single, well-controlled irradiation setting (ADR = 240 Gy/s with fixed pulse structure). Systematic

investigation of dose-per-pulse, pulse repetition frequency, and temporal microstructure will require dedicated radiophysics-biology studies beyond the scope of the present work. Importantly, the same irradiation platform and closely related FLASH/UHDR configurations have already been successfully employed in previous *in vitro* and in *vivo* studies from our consortium, including reports demonstrating preservation of systemic and tissue homeostasis with maintained antitumor efficacy (79), mitigation of radiation-induced damage in healthy bronchial epithelial cells (80), and differential FLASH responses in retinal pigment epithelial models both *in vitro* and *in vivo* (43). Together, these studies support the robustness, reproducibility, and biological relevance of the irradiation conditions used here.

The differential activation of senescence and metabolic remodeling also suggests potential synergy with senolytic or metabolism-targeted therapies. Given the urgent need to improve therapeutic windows in GBM, where dose escalation is limited by neurotoxicity, our findings support further development of UHDR/FLASH approaches in glioblastoma. Importantly, the present study was not designed to recapitulate the canonical *in vivo* FLASH effect, but rather to define early cell-intrinsic responses induced under tightly controlled FLASH/UHDR conditions. Accordingly, these findings should not be interpreted as direct evidence of long-term tissue sparing, but as mechanistic insight into early biological processes triggered by UHDR irradiation. Our data indicate that FLASH/UHDR exposure induces cell-type-specific redox-metabolic reprogramming, characterized by relative preservation of mitochondrial function in healthy astrocytes and sustained metabolic stress in glioma cells. Many of the mechanistic readouts employed here, including real-time bioenergetic profiling, redox-sensitive flow cytometry, mitochondrial membrane potential, and dynamic metabolic analyses, remain technically achievable and interpretable only in controlled *in vitro* systems, which therefore continue to represent essential platforms for mechanistic radiobiology studies. Future investigations using patient-derived glioblastoma models, advanced three-dimensional systems, and *in vivo* FLASH paradigms will be necessary to determine whether the redox–metabolic signatures identified here are maintained in clinically relevant tumor microenvironments and contribute to FLASH-associated biological responses.

Declaration of Interests

The authors declare that the research was conducted in the absence of any commercial or financial relationships that could be construed as a potential conflict of interest.

Supporting Data Statement

Supporting Data generated and/or analyzed during the current study are available from the corresponding author upon reasonable request.

Acknowledgements and Funding

We thank Ms. Elena Novelli, Vania Liverani and Renzo di Renzo for excellent technical support. This work was generously supported through grants from Finanziato dall'Unione europea- Next Generation EU, Missione 4 Componente 1 CUP I53D23001020001 to E.C. and B.D., Intesa SanPaolo B/2025/0257 to B.D., and Piano Nazionale di Ripresa e Resilienza (PNRR), Missione 4, Componente 2, Ecosistemi dell'Innovazione - Tuscany Health Ecosystem (THE), Project no. ECS_00000017; CUP I53C22000780001, spoke 1 "Advanced Radiotherapies and Diagnostics in Oncology" to B. D and M.C. We also thank Fondazione Pisa for funding CPFR with the grant "prog. n. 134/2021". Additional support was provided by AIRC under AIRC #IG 2024 ID-30434 project to M.C.

Author Contribution

G.R., E.DS., R.N., and B.D. designed the study. G.R., E.DS., R.N., M.P., F.R., S.B., A.C., F.P., F.DM. and B.D. designed and performed experiments. G.R., E.DS., R.N., M.P., F.R., S.B., E.C., A.C., F.DM., E.V., M.C. and B.D. analyzed and interpreted data. G.R. and B.D. wrote the manuscript. E.C., B.D. and M.C. acquired funding.

References

1. Favaudon V, Caplier L, Monceau V, Pouzoulet F, Sayarath M, Fouillade C, et al. Ultrahigh dose-rate FLASH irradiation increases the differential response between normal and tumor tissue in mice. Sci Transl Med. 2014 Jul 16;6(245):245ra93. doi:10.1126/scitranslmed.3008973 PubMed PMID: 25031268.
2. Guo Y, Hao S, Huang Q, Di C, Gan L, Xie Y, et al. Unraveling the dual nature of FLASH radiotherapy: From normal tissue sparing to tumor control. Cancer Lett. 2025 Oct;630:217895. doi:10.1016/j.canlet.2025.217895
3. Durante M, Loeffler JS. Charged particles in radiation oncology. Nat Rev Clin Oncol. 2010 Jan;7(1):37–43. doi:10.1038/nrclinonc.2009.183 PubMed PMID: 19949433.
4. Chow JCL, Ruda HE. Mechanisms of Action in FLASH Radiotherapy: A Comprehensive Review of Physicochemical and Biological Processes on Cancerous and Normal Cells. Cells. 2024 May 14;13(10). doi:10.3390/cells13100835 PubMed PMID: 38786057.

5. Bourhis J, Montay-Gruel P, Gonçalves Jorge P, Bailat C, Petit B, Ollivier J, et al. Clinical translation of FLASH radiotherapy: Why and how? Radiother Oncol. 2019 Oct;139:11–7. doi:10.1016/j.radonc.2019.04.008 PubMed PMID: 31253466.
6. Ward JF. DNA damage produced by ionizing radiation in mammalian cells: identities, mechanisms of formation, and reparability. Prog Nucleic Acid Res Mol Biol. 1988;35:95–125. doi:10.1016/s0079-6603(08)60611-x PubMed PMID: 3065826.
7. Schieber M, Chandel NS. ROS Function in Redox Signaling and Oxidative Stress. Current Biology. 2014 May;24(10):R453–62. doi:10.1016/j.cub.2014.03.034
8. Rosini G, Ciarrocchi E, D'Orsi B. Mechanisms of the FLASH effect: current insights and advances. Front Cell Dev Biol. 2025 May 9;13. doi:10.3389/fcell.2025.1575678
9. Bogaerts E, Macaeva E, Isebaert S, Haustermans K. Potential Molecular Mechanisms behind the Ultra-High Dose Rate "FLASH" Effect. Int J Mol Sci. 2022 Oct 11;23(20):12109. doi:10.3390/ijms232012109
10. Montay-Gruel P, Acharya MM, Petersson K, Alikhani L, Yakkala C, Allen BD, et al. Long-term neurocognitive benefits of FLASH radiotherapy driven by reduced reactive oxygen species. Proc Natl Acad Sci U S A. 2019 May 28;116(22):10943–51. doi:10.1073/pnas.1901777116 PubMed PMID: 31097580.
11. Spitz DR, Buettner GR, Petronek MS, St-Aubin JJ, Flynn RT, Waldron TJ, et al. An integrated physico-chemical approach for explaining the differential impact of FLASH versus conventional dose rate irradiation on cancer and normal tissue responses. Radiother Oncol. 2019 Oct;139:23–7. doi:10.1016/j.radonc.2019.03.028 PubMed PMID: 31010709.
12. Tang R, Yin J, Liu Y, Xue J. FLASH radiotherapy: A new milestone in the field of cancer radiotherapy. Cancer Lett. 2024 Apr;587:216651. doi:10.1016/j.canlet.2024.216651
13. Geirnaert F, Kerkhove L, Montay-Gruel P, Gevaert T, Dufait I, De Ridder M. Exploring the Metabolic Impact of FLASH Radiotherapy. Cancers (Basel). 2025 Jan 3;17(1):133. doi:10.3390/cancers17010133
14. DeBerardinis RJ, Chandel NS. Fundamentals of cancer metabolism. Sci Adv. 2016 May;2(5):e1600200. doi:10.1126/sciadv.1600200 PubMed PMID: 27386546.
15. Pavlova NN, Zhu J, Thompson CB. The hallmarks of cancer metabolism: Still emerging. Cell Metab. 2022 Mar 1;34(3):355–77. doi:10.1016/j.cmet.2022.01.007 PubMed PMID: 35123658.
16. Warburg O. On the Origin of Cancer Cells. Science (1979). 1956 Feb 24;123(3191):309–14. doi:10.1126/science.123.3191.309
17. Ward PS, Thompson CB. Metabolic reprogramming: a cancer hallmark even warburg did not anticipate. Cancer Cell. 2012 Mar 20;21(3):297–308. doi:10.1016/j.ccr.2012.02.014 PubMed PMID: 22439925.

18. Stupp R, Mason WP, van den Bent MJ, Weller M, Fisher B, Taphoorn MJB, et al. Radiotherapy plus concomitant and adjuvant temozolomide for glioblastoma. N Engl J Med. 2005 Mar 10;352(10):987–96. doi:10.1056/NEJMoa043330 PubMed PMID: 15758009.

19. Singh S, Dey D, Barik D, Mohapatra I, Kim S, Sharma M, et al. Glioblastoma at the crossroads: current understanding and future therapeutic horizons. Signal Transduct Target Ther. 2025 Jul 9;10(1):213. doi:10.1038/s41392-025-02299-4

20. Tini P, Donnini F, Marampon F, Pastina P, Rubino G, Battaglia G, et al. Timing matters: overall treatment time, radiotherapy interruptions, and outcomes in glioblastomas—prognostic significance in different biological sub-groups. J Neurooncol. 2025 Dec 25;175(3):1261–9. doi:10.1007/s11060-025-05215-6

21. Quail DF, Joyce JA. The Microenvironmental Landscape of Brain Tumors. Cancer Cell. 2017 Mar 13;31(3):326–41. doi:10.1016/j.ccell.2017.02.009 PubMed PMID: 28292436.

22. DeCordova S, Shastri A, Tsolaki AG, Yasmin H, Klein L, Singh SK, et al. Molecular Heterogeneity and Immunosuppressive Microenvironment in Glioblastoma. Front Immunol. 2020 Jul 17;11. doi:10.3389/fimmu.2020.01402

23. Szatmári T, Lumniczky K, Désaknai S, Trajcevski S, Hídvégi EJ, Hamada H, et al. Detailed characterization of the mouse glioma 261 tumor model for experimental glioblastoma therapy. Cancer Sci. 2006 Jun;97(6):546–53. doi:10.1111/j.1349-7006.2006.00208.x PubMed PMID: 16734735.

24. Bourhis J, Montay-Gruel P, Gonçalves Jorge P, Bailat C, Petit B, Ollivier J, et al. Clinical translation of FLASH radiotherapy: Why and how? Radiother Oncol. 2019 Oct;139:11–7. doi:10.1016/j.radonc.2019.04.008 PubMed PMID: 31253466.

25. Limoli CL, Vozenin MC. Reinventing Radiobiology in the Light of FLASH Radiotherapy. Annu Rev Cancer Biol. 2023 Apr;7:1–21. doi:10.1146/annurev-cancerbio-061421-022217 PubMed PMID: 39421564.

26. Di Martino F, Del Sarto D, Bass G, Capaccioli S, Celentano M, Coves D, et al. Architecture, flexibility and performance of a special electron linac dedicated to Flash radiotherapy research: electronFlash with a triode gun of the centro pisano flash radiotherapy (CPFR). Front Phys. 2023 Nov 16;11. doi:10.3389/fphy.2023.1268310

27. Marinelli M, Felici G, Galante F, Gasparini A, Giuliano L, Heinrich S, et al. Design, realization, and characterization of a novel diamond detector prototype for FLASH radiotherapy dosimetry. Med Phys. 2022 Mar;49(3):1902–10. doi:10.1002/mp.15473 PubMed PMID: 35064594.

28. Di Martino F, Del Sarto D, Barone S, Giuseppina Bisogni M, Capaccioli S, Galante F, et al. A new calculation method for the free electron fraction of an ionization chamber in the ultra-high-dose-per-pulse regimen. Physica Medica. 2022 Nov;103:175–80. doi:10.1016/j.ejmp.2022.11.001

29. Di Martino F, Del Sarto D, Giuseppina Bisogni M, Capaccioli S, Galante F, Gasperini A, et al. A new solution for UHDP and UHDR (Flash) measurements: Theory and conceptual design of ALLS chamber. Physica Medica. 2022 Oct;102:9–18. doi:10.1016/j.ejmp.2022.08.010

30. Di Martino F, Barca P, Barone S, Bortoli E, Borgheresi R, De Stefano S, et al. FLASH Radiotherapy With Electrons: Issues Related to the Production, Monitoring, and Dosimetric Characterization of the Beam. Front Phys. 2020 Nov 2;8. doi:10.3389/fphy.2020.570697

31. Del Sarto D, Masturzo L, Cavalieri A, Celentano M, Fuentes T, Gadducci G, et al. A systematic investigation on the response of EBT-XD gafchromic films to varying dose-per-pulse, average dose-rate and instantaneous dose-rate in electron flash beams. Front Phys. 2025 Apr 29;13. doi:10.3389/fphy.2025.1474416

32. Ciarrocchi E, Ravera E, Cavalieri A, Celentano M, Del Sarto D, Di Martino F, et al. Plastic scintillator-based dosimeters for ultra-high dose rate (UHDR) electron radiotherapy. Physica Medica. 2024 May;121:103360. doi:10.1016/j.ejmp.2024.103360

33. Gómez F, Gonzalez-Castaño DM, Fernández NG, Pardo-Montero J, Schüller A, Gasparini A, et al. Development of an ultra-thin parallel plate ionization chamber for dosimetry in FLASH radiotherapy. Med Phys. 2022 Jul;49(7):4705–14. doi:10.1002/mp.15668 PubMed PMID: 35416306.

34. Milluzzo G, De Napoli M, Di Martino F, Amato A, Del Sarto D, D'Oca MC, et al. Comprehensive dosimetric characterization of novel silicon carbide detectors with UHDR electron beams for FLASH radiotherapy. Med Phys. 2024 Sep 21;51(9):6390–401. doi:10.1002/mp.17172

35. Cova F, Morrocchi M, Fasoli M, Ciarrocchi E, Pensavalle JH, Gallo S, et al. Stem effect-free (Y,Yb)AG-based detectors for ultra-high dose rate electron beam dosimetry. Sens Actuators A Phys. 2025 Aug;390:116539. doi:10.1016/j.sna.2025.116539

36. Meir EG, editor. CNS Cancer. Totowa, NJ: Humana Press; 2009. doi:10.1007/978-1-60327-553-8

37. Vannini E, Panighini A, Cerri C, Fabbri A, Lisi S, Pracucci E, et al. The bacterial protein toxin, cytotoxic necrotizing factor 1 (CNF1) provides long-term survival in a murine glioma model. BMC Cancer. 2014 Dec 18;14(1):449. doi:10.1186/1471-2407-14-449

38. PONTÉN J, MACINTYRE EH. LONG TERM CULTURE OF NORMAL AND NEOPLASTIC HUMAN GLIA. Acta Pathologica Microbiologica Scandinavica. 1968 Sep 18;74(4):465–86. doi:10.1111/j.1699-0463.1968.tb03502.x

39. Scuderi SA, Ardizzone A, Mannino D, Palermo N, De Luca F, Catalfamo A, et al. Modulation of Wnt/β-Catenin Pathway by Aesculus hippocastanum Extract Enhances Temozolomide Sensitivity in Glioblastoma Cells. J Cell Mol Med. 2026 Feb;30(4):e70979. doi:10.1111/jcmm.70979 PubMed PMID: 41693444.

40. Iovino L, Giusti V, Pischedda F, Giusto E, Plotegher N, Marte A, et al. Trafficking of the glutamate transporter is impaired in LRRK2-related Parkinson's disease. Acta Neuropathol. 2022 Jul;144(1):81–106. doi:10.1007/s00401-022-02437-0 PubMed PMID: 35596783.

41. Streubel-Gallasch L, Giusti V, Sandre M, Tessari I, Plotegher N, Giusto E, et al. Parkinson's Disease-Associated LRRK2 Interferes with Astrocyte-Mediated Alpha-Synuclein Clearance. Mol Neurobiol. 2021 Jul;58(7):3119–40. doi:10.1007/s12035-021-02327-8 PubMed PMID: 33629273.

42. Kealey J, Düssmann H, Llorente-Folch I, Niewidok N, Salvucci M, Prehn JHM, et al. Effect of TP53 deficiency and KRAS signaling on the bioenergetics of colon cancer cells in response to different substrates: A single cell study. Front Cell Dev Biol. 2022;10:893677. doi:10.3389/fcell.2022.893677 PubMed PMID: 36238683.

43. Di Marco B, Sansevero G, D'Orsi B, De Santis E, Salamone G, Cavalieri A, et al. Unraveling the effects of FLASH and conventional irradiation on retinal pigment epithelial cells: in vitro and in vivo studies. Sci Rep. 2025 Jul 2;15(1):22938. doi:10.1038/s41598-025-06101-x PubMed PMID: 40594566.

44. Montay-Gruel P, Petersson K, Jaccard M, Boivin G, Germond JF, Petit B, et al. Irradiation in a flash: Unique sparing of memory in mice after whole brain irradiation with dose rates above 100Gy/s. Radiother Oncol. 2017 Sep;124(3):365–9. doi:10.1016/j.radonc.2017.05.003 PubMed PMID: 28545957.

45. Vozenin MC, Hendry JH, Limoli CL. Biological Benefits of Ultra-high Dose Rate FLASH Radiotherapy: Sleeping Beauty Awoken. Clin Oncol (R Coll Radiol). 2019 Jul;31(7):407–15. doi:10.1016/j.clon.2019.04.001 PubMed PMID: 31010708.

46. Vozenin MC, Montay-Gruel P, Tsoutsou P, Limoli CL. Mechanisms, challenges and opportunities for FLASH radiotherapy in cancer. Nat Rev Cancer. 2025 Oct 24. doi:10.1038/s41568-025-00878-9

47. Simmons DA, Lartey FM, Schüler E, Rafat M, King G, Kim A, et al. Reduced cognitive deficits after FLASH irradiation of whole mouse brain are associated with less hippocampal dendritic spine loss and neuroinflammation. Radiotherapy and Oncology. 2019 Oct;139:4–10. doi:10.1016/j.radonc.2019.06.006

48. Ni H, Reitman ZJ, Zou W, Akhtar MN, Paul R, Huang M, et al. FLASH radiation reprograms lipid metabolism and macrophage immunity and sensitizes medulloblastoma to CAR-T cell therapy. Nat Cancer. 2025 Mar;6(3):460–73. doi:10.1038/s43018-025-00905-6 PubMed PMID: 39910249.

49. Montay-Gruel P, Acharya MM, Petersson K, Alikhani L, Yakkala C, Allen BD, et al. Long-term neurocognitive benefits of FLASH radiotherapy driven by reduced reactive oxygen species. Proc Natl Acad Sci U S A. 2019 May 28;116(22):10943–51. doi:10.1073/pnas.1901777116 PubMed PMID: 31097580.

50. Campisi J. Aging, cellular senescence, and cancer. Annu Rev Physiol. 2013;75:685–705. doi:10.1146/annurev-physiol-030212-183653 PubMed PMID: 23140366.

51. Rodier F, Campisi J. Four faces of cellular senescence. J Cell Biol. 2011 Feb 21;192(4):547–56. doi:10.1083/jcb.201009094 PubMed PMID: 21321098.

52. Pratx G, Kapp DS. Ultra-High-Dose-Rate FLASH Irradiation May Spare Hypoxic Stem Cell Niches in Normal Tissues. Int J Radiat Oncol Biol Phys. 2019 Sep 1;105(1):190–2. doi:10.1016/j.ijrobp.2019.05.030 PubMed PMID: 31145965.

53. Morgan WF, Sowa MB. Non-targeted effects induced by ionizing radiation: mechanisms and potential impact on radiation induced health effects. Cancer Lett. 2015 Jan 1;356(1):17–21. doi:10.1016/j.canlet.2013.09.009 PubMed PMID: 24041870.

54. Mothersill C, Seymour C. Radiation-induced bystander effects: past history and future directions. Radiat Res. 2001 Jun;155(6):759–67. doi:10.1667/0033-7587(2001)155[0759:ribeph]2.0.co;2 PubMed PMID: 11352757.

55. Hei TK, Zhou H, Ivanov VN, Hong M, Lieberman HB, Brenner DJ, et al. Mechanism of radiation-induced bystander effects: a unifying model. Journal of Pharmacy and Pharmacology. 2008 Aug 1;60(8):943–50. doi:10.1211/jpp.60.8.0001

56. Ghadimi K, Abbas I, Karandish A, Crisman C, Eskandar EN, Kobets AJ. Cognitive Decline in Glioblastoma (GB) Patients with Different Treatment Modalities and Insights on Untreated Cases. Curr Oncol. 2025 Mar 6;32(3). doi:10.3390/curroncol32030152 PubMed PMID: 40136356.

57. Girdhani S, Abel E, Katsis A, Rodriquez A, Senapati S, KuVillanueva A, et al. Abstract LB-280: FLASH: A novel paradigm changing tumor irradiation platform that enhances therapeutic ratio by reducing normal tissue toxicity and activating immune pathways. Cancer Res. 2019 Jul 1;79(13_Supplement):LB-280-LB-280. doi:10.1158/1538-7445.AM2019-LB-280

58. Fouillade C, Curras-Alonso S, Giuranno L, Quelennec E, Heinrich S, Bonnet-Boissinot S, et al. FLASH Irradiation Spares Lung Progenitor Cells and Limits the Incidence of Radio-induced Senescence. Clinical Cancer Research. 2020 Mar 15;26(6):1497–506. doi:10.1158/1078-0432.CCR-19-1440

59. Andrabi SA, Kim NS, Yu SW, Wang H, Koh DW, Sasaki M, et al. Poly(ADP-ribose) (PAR) polymer is a death signal. Proceedings of the National Academy of Sciences. 2006 Nov 28;103(48):18308–13. doi:10.1073/pnas.0606526103

60. Favaudon V, Caplier L, Monceau V, Pouzoulet F, Sayarath M, Fouillade C, et al. Ultrahigh dose-rate FLASH irradiation increases the differential response between normal and tumor tissue in mice. Sci Transl Med. 2014 Jul 16;6(245):245ra93. doi:10.1126/scitranslmed.3008973 PubMed PMID: 25031268.

61. Adrian G, Konradsson E, Lempart M, Bäck S, Ceberg C, Petersson K. The FLASH effect depends on oxygen concentration. Br J Radiol. 2020 Feb 1;93(1106):20190702. doi:10.1259/bjr.20190702 PubMed PMID: 31825653.

62. Chow JCL, Ruda HE. Mechanisms of Action in FLASH Radiotherapy: A Comprehensive Review of Physicochemical and Biological Processes on Cancerous and Normal Cells. Cells. 2024 May 14;13(10). doi:10.3390/cells13100835 PubMed PMID: 38786057.

63. de Kruijff RM. FLASH radiotherapy: ultra-high dose rates to spare healthy tissue. Int J Radiat Biol. 2020 Apr;96(4):419–23. doi:10.1080/09553002.2020.1704912 PubMed PMID: 31829765.

64. McGarrigle JM, Long KR, Prezado Y. The FLASH effect-an evaluation of preclinical studies of ultra-high dose rate radiotherapy. Front Oncol. 2024;14:1340190. doi:10.3389/fonc.2024.1340190 PubMed PMID: 38711846.

65. Vozenin MC, Montay-Gruel P, Limoli C, Germond JF. All Irradiations that are Ultra-High Dose Rate may not be FLASH: The Critical Importance of Beam Parameter Characterization and In Vivo Validation of the FLASH Effect. Radiat Res. 2020 Dec 1;194(6):571–2. doi:10.1667/RADE-20-00141.1 PubMed PMID: 32853355.

66. Buonanno M, Grilj V, Brenner DJ. Biological effects in normal cells exposed to FLASH dose rate protons. Radiother Oncol. 2019 Oct;139:51–5. doi:10.1016/j.radonc.2019.02.009 PubMed PMID: 30850209.

67. Loo BW, Schuler E, Lartey FM, Rafat M, King GJ, Trovati S, et al. (P003) Delivery of Ultra-Rapid Flash Radiation Therapy and Demonstration of Normal Tissue Sparing After Abdominal Irradiation of Mice. International Journal of Radiation Oncology*Biology*Physics. 2017 Jun;98(2):E16. doi:10.1016/j.ijrobp.2017.02.101

68. Zhang Z, Liu X, Chen D, Yu J. Radiotherapy combined with immunotherapy: the dawn of cancer treatment. Signal Transduct Target Ther. 2022 Jul 29;7(1):258. doi:10.1038/s41392-022-01102-y PubMed PMID: 35906199.

69. Montay-Gruel P, Acharya MM, Gonçalves Jorge P, Petit B, Petridis IG, Fuchs P, et al. Hypofractionated FLASH-RT as an Effective Treatment against Glioblastoma that Reduces Neurocognitive Side Effects in Mice. Clin Cancer Res. 2021 Feb 1;27(3):775–84. doi:10.1158/1078-0432.CCR-20-0894 PubMed PMID: 33060122.

70. Spitz DR, Buettner GR, Petronek MS, St-Aubin JJ, Flynn RT, Waldron TJ, et al. An integrated physico-chemical approach for explaining the differential impact of FLASH versus conventional dose rate irradiation on cancer and normal tissue responses. Radiother Oncol. 2019 Oct;139:23–7. doi:10.1016/j.radonc.2019.03.028 PubMed PMID: 31010709.

71. Morrow D, Minami J, Nathanson DA. Metabolic Vulnerabilities in Brain Cancer. Neurosurg Clin N Am. 2021 Apr;32(2):159–69. doi:10.1016/j.nec.2020.12.006

72. Tong X, Tang R, Xiao M, Xu J, Wang W, Zhang B, et al. Targeting cell death pathways for cancer therapy: recent developments in necroptosis, pyroptosis, ferroptosis, and cuproptosis research. J Hematol Oncol. 2022 Dec 8;15(1):174. doi:10.1186/s13045-022-01392-3 PubMed PMID: 36482419.

73. Esteban-Román NF, Taddei E, Castro-Velázquez E, Villafuentes-Vidal L, Velez-Herrera A, Rubio-Osornio M, et al. Redox-Regulated Pathways in Glioblastoma Stem-like Cells: Mechanistic Insights and Therapeutic Implications. Brain Sci. 2025 Aug 19;15(8). doi:10.3390/brainsci15080884 PubMed PMID: 40867215.

74. Huszthy PC, Daphu I, Niclou SP, Stieber D, Nigro JM, Sakariassen PØ, et al. In vivo models of primary brain tumors: pitfalls and perspectives. Neuro Oncol. 2012 Aug;14(8):979–93. doi:10.1093/neuonc/nos135 PubMed PMID: 22679124.

75. Allen M, Bjerke M, Edlund H, Nelander S, Westermark B. Origin of the U87MG glioma cell line: Good news and bad news. Sci Transl Med. 2016 Aug 31;8(354):354re3. doi:10.1126/scitranslmed.aaf6853 PubMed PMID: 27582061.

76. Kartini DA, Karoon P, Malad Y, Tippayamontri T, Sanghangthum T, Talabnin C, et al. Human glioblastoma (U87) cells grown in 3D culture showed a radio-resistance to X-ray and proton radiation. Radiol Phys Technol. 2025 Sep 13;18(3):688–97. doi:10.1007/s12194-025-00921-2

77. Miki K, Yagi M, Yoshimoto K, Kang D, Uchiumi T. Mitochondrial dysfunction and impaired growth of glioblastoma cell lines caused by antimicrobial agents inducing ferroptosis under glucose starvation. Oncogenesis. 2022 Oct 4;11(1):59. doi:10.1038/s41389-022-00437-z

78. Murata MM, Kong X, Moncada E, Chen Y, Imamura H, Wang P, et al. NAD+ consumption by PARP1 in response to DNA damage triggers metabolic shift critical for damaged cell survival. Mol Biol Cell. 2019 Sep 15;30(20):2584–97. doi:10.1091/mbc.E18-10-0650 PubMed PMID: 31390283.

79. Furini G, Mota da Silva E, Usai A, Scabia G, Kusmic C, Faita F, et al. FLASH radiotherapy preserves systemic and tissue homeostasis while maintaining antitumor efficacy. BMC Med. 2026 Feb 26;24(1). doi:10.1186/s12916-026-04724-z PubMed PMID: 41742130.

80. Del Debbio F, Bertilacchi MS, Cavalieri A, Gadducci G, Giannini N, Gonnelli A, et al. Mitigating the side effects of conventional radiotherapy: deep examination of the FLASH effect on human healthy bronchial epithelial cell line. Cancer Treat Res Commun. 2025;44:100961. doi:10.1016/j.ctarc.2025.100961 PubMed PMID: 40651227.

Figure Legends

Fig. 1 FLASH-RT reduces ROS accumulation and cell death while sustaining senescence markers in healthy astrocytes (a) Experimental setup for intracellular ROS measurement using the DCFDA assay. (b, c) Real-time monitoring of intracellular ROS in healthy astrocytes following 8 Gy FLASH- or CONV-RT, expressed as fold change relative to the baseline. FLASH induced a rapid ROS increase (b), with a significantly lower peak compared with CONV (c). Data are mean ± SEM (n = 3 independent experiments). *p < 0.05 *vs* Control; #p < 0.05 FLASH *vs* CONV (one-way ANOVA followed by Tukey's post hoc test). (d) Quantification of cell death at 72 h post-irradiation. Data are mean ± SEM (n = 3 independent experiments). *p < 0.05 *vs* Control; #p < 0.05 FLASH *vs* CONV (one-way ANOVA followed by Tukey's post hoc test). (e) Representative Hoechst (blue) and DIC images of Control, FLASH- and CONV-irradiated astrocytic cells at 72 h. Cell death was assessed by nuclear condensation and fragmentation. Three subfields per well (100 - 150 cells each), n = 9 wells/condition from 3 independent cultures. Scale bar: 20 µm. (f) qRT-PCR analysis of senescence markers *p53, p21* and *p16* at indicated time points after irradiation. Data are mean ± SEM (n = 3 independent experiments). *p < 0.05 *vs* Control; #p < 0.05 FLASH *vs* CONV (one-way ANOVA followed by Tukey's post hoc test).

Fig. 2 FLASH-RT induces prolonged ROS accumulation and transcriptional activation of stress- and autophagy-related pathways in GL261 cells, accompanied by G2/M accumulation (a - c) Real-time ROS analysis after 8 Gy FLASH- or CONV-RT. FLASH induced a lower early ROS peak (b) but a higher rate of ROS accumulation over time (c). Data are mean ± SEM (n = 3 independent experiments). *p < 0.05 *vs* Control; #p < 0.05 FLASH *vs* CONV (one-way ANOVA followed by Tukey's post hoc test). (d) Flow cytometry analysis of Annexin V staining, expressed as percentage of Annexin V-fluorescence relative to control, 72 h after 8 Gy FLASH- or CONV-RT. Data are mean ± SEM (n = 3 independent experiments). *p < 0.05 *vs* Control; #p < 0.05 FLASH *vs* CONV (two-way ANOVA followed by Tukey's post hoc test). (e - g) qRT-PCR analysis of genes involved in apoptosis (*Bax, Bcl-2*), senescence (*p53, p21, p16*), and autophagy (*LC3, Beclin1*) at 0 - 72 h after 8 Gy irradiation. FLASH induced earlier and stronger transcriptional activation of stress-response pathways compared with CONV. Data are mean ± SEM (n = 3 independent experiments). *p < 0.05 *vs* Control; #p < 0.05 FLASH *vs* CONV (two-way ANOVA followed by Tukey's post hoc test). (h - i) Cell cycle analysis by PI staining using flow cytometry. Data are expressed as the percentage of PI fluorescence in each phase of the cell cycle, 24 h and 72 h after 8 Gy FLASH- or CONV-RT. Data are mean ± SEM (n = 3 independent experiments). *p < 0.05 *vs* Control; #p < 0.05 FLASH *vs* CONV (two-way ANOVA followed by Tukey's post hoc test).

Fig. 3 FLASH irradiation preserves mitochondrial function in healthy astrocytes while inducing mitochondrial dysfunction and ROS accumulation in GL261 cells (a - h) Flow cytometry analysis of mitochondrial mass (MitoTracker Green; a, e), active mitochondria (MitoTracker Red CMXROS; b, f), mitochondrial membrane potential (TMRM; c, g), and intracellular ROS (CellROX; d, h) in healthy astrocytes and GL261 cells at 0 - 72 h after 8 Gy FLASH- or CONV-RT. Data are normalized to baseline control. Data are mean ± SEM (n = 3 independent experiments). *p < 0.05 *vs* baseline (0); #p < 0.05 between conditions; $p < 0.05 FLASH *vs* CONV (two-way ANOVA followed by Tukey's post hoc test). Heat maps summarize the flow cytometry-based measurements in healthy astrocytes and GL261 glioma cells following FLASH- or CONV-RT, highlighting the temporal evolution of mitochondrial and oxidative stress responses. Color intensity represents relative normalized signal intensity, with increasing values indicated by a yellow-to-green color gradient.

Fig. 4 FLASH-RT preserves mitochondrial bioenergetic flexibility in healthy astrocytes with limited contribution of regulated cell death pathways Seahorse XF extracellular flux analysis of mitochondrial respiration in healthy astrocytes (a -e) following FLASH- or CONV-RT, performed in the absence or presence of pharmacological inhibitors (DPQ, zVAD, Nec-1, and Calpeptin) targeting distinct cell death pathways. Mitochondrial bioenergetic parameters include basal respiration (BR), ATP-linked respiration, maximal respiration (MR), spare respiratory capacity (SRC), non-mitochondrial respiration (NMR), and proton leak. Data are presented as mean ± SEM (n = 3 - 4 independent experiments). *p < 0.05 *vs* Control; #p < 0.05 FLASH *vs* CONV (one-way ANOVA followed by Tukey's post hoc test). Heat maps summarize the Seahorse extracellular flux measurements obtained in healthy astrocytes after FLASH- or CONV-RT, in the absence or presence of pharmacological inhibitors. Color intensity represents relative normalized metabolic activity, with increasing values indicated by a yellow-to-green gradient, highlighting metabolic differences between irradiation modalities and pathway inhibition conditions.

Fig. 5 FLASH-RT induces persistent mitochondrial respiratory suppression in GL261 glioma cells with contributions from multiple regulated cell death pathways Seahorse XF extracellular flux analysis of mitochondrial respiration in GL261 cells (a - f) following FLASH- or CONV-RT, performed in the absence or presence of pharmacological inhibitors (DPQ, zVAD, Nec-1, and Calpeptin) targeting distinct cell death pathways. Data are presented as mean ± SEM (n = 3 - 4 independent experiments). *p < 0.05 *vs* Control; #p < 0.05 FLASH *vs* CONV (one-way ANOVA followed by Tukey's post hoc test). Heat maps summarize the Seahorse extracellular flux measurements obtained in GL261 cells after FLASH- or CONV-RT, in the absence or presence of pharmacological inhibitors. Color intensity represents

relative normalized metabolic activity, with increasing values indicated by a yellow-to-green gradient, highlighting differences in mitochondrial metabolism between irradiation modalities and pathway inhibition conditions.

Fig. 6 FLASH-RT enhances oxidative stress and impairs mitochondrial bioenergetics in human U87 glioma cells (a) Flow cytometry analysis of Annexin V staining in U87 cells, expressed as percentage of Annexin V fluorescence relative to control, 72 h after 8 Gy FLASH- or CONV-RT. Data are mean ± SEM (n = 3 independent experiments). *p < 0.05 *vs* Control; #p < 0.05 FLASH *vs* CONV (one-way ANOVA followed by Tukey's post hoc test). (b, c) Flow cytometry analysis of mitochondrial membrane potential (TMRM; b) and intracellular ROS (CellROX; c) in U87 glioblastoma cells at 0 - 72 h after 8 Gy FLASH- or CONV-RT. Data are normalized to baseline Control. Data are mean ± SEM (n = 3 independent experiments). *p < 0.05 *vs* baseline (0); #p < 0.05 between conditions; $p < 0.05 FLASH *vs* CONV (two-way ANOVA followed by Tukey's post hoc test). (d) Quantification of intracellular ATP levels in U87 cells at 0, 2, 24 h after 8 Gy FLASH- or CONV-RT. Data are normalized to protein content. Data are mean ± SEM (n = 3 independent experiments). *p < 0.05 *vs* baseline (0); #p < 0.05 *vs* Control; $p < 0.05 FLASH *vs* CONV (two-way ANOVA followed by Tukey's post hoc test). (e) Quantification of intracellular NAD^+ levels in U87 cells at 0, 2, 24 h after 8 Gy FLASH- or CONV-RT. Data are normalized to protein content. *p < 0.05 *vs* baseline (0); #p < 0.05 *vs* Control; $p < 0.05 FLASH *vs* CONV (two-way ANOVA followed by Tukey's post hoc test). (f) Seahorse XF extracellular flux analysis of mitochondrial respiration in U87 cells following 8 Gy of FLASH- or CONV-RT. Data are presented as mean ± SEM (n = 3 - 4 independent experiments). *p < 0.05 *vs* Control; #p < 0.05 FLASH *vs* CONV (one-way ANOVA followed by Tukey's post hoc test).

Figures

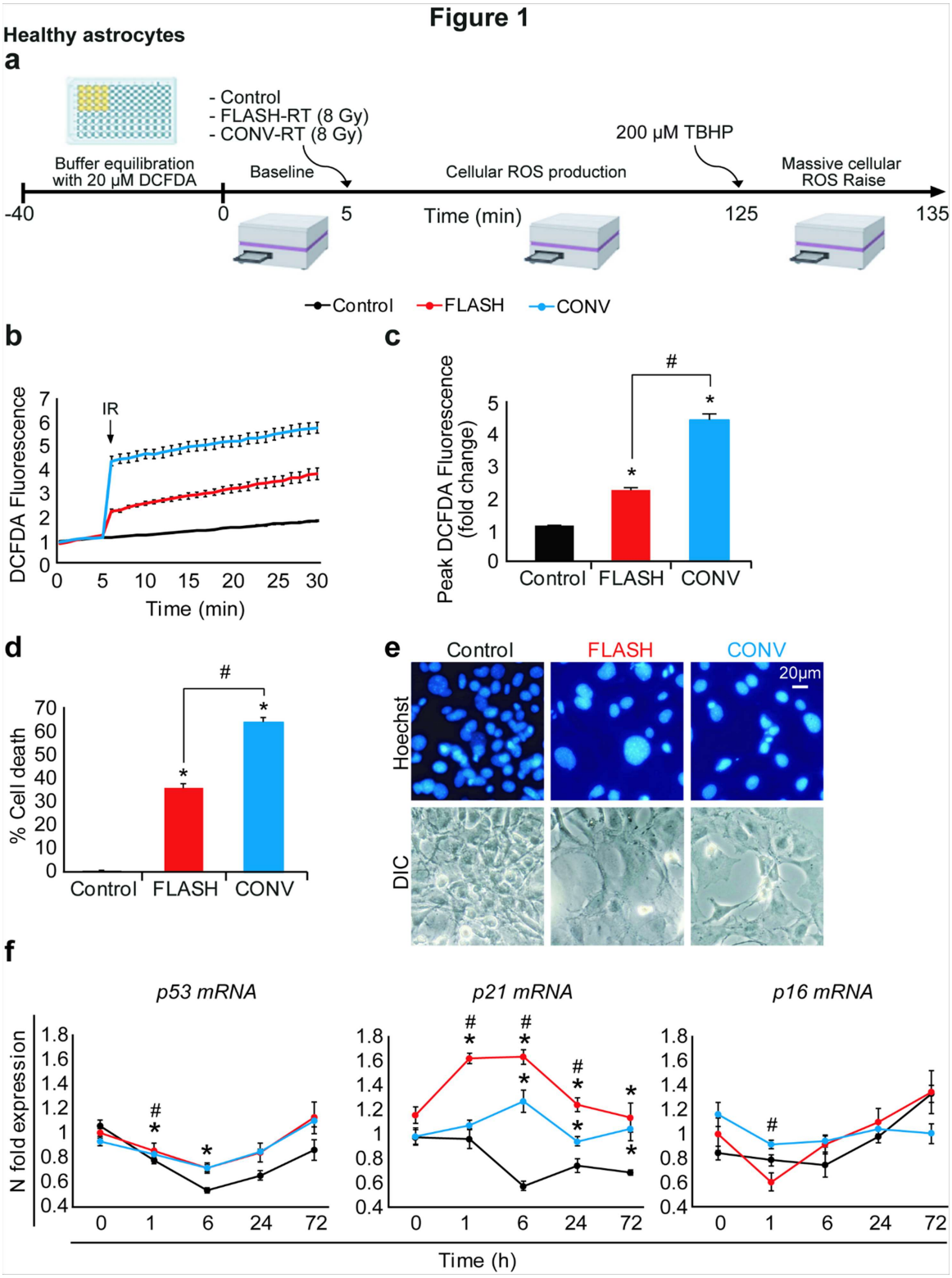


Figure 1

FLASH-RT reduces ROS accumulation and cell death while sustaining senescence markers in healthy astrocytes (a) Experimental setup for intracellular ROS measurement using the DCFDA assay. (b, c) Real-time monitoring of intracellular ROS in healthy astrocytes following 8 Gy FLASH- or CONV-RT, expressed

as fold change relative to the baseline. FLASH induced a rapid ROS increase (b), with a significantly lower peak compared with CONV (c). Data are mean ± SEM (n = 3 independent experiments). *p < 0.05 *vs*Control; #p < 0.05 FLASH *vs* CONV (one-way ANOVA followed by Tukey's post hoc test). (d) Quantification of cell death at 72 h post-irradiation. Data are mean ± SEM (n = 3 independent experiments). *p < 0.05 *vs*Control; #p < 0.05 FLASH *vs* CONV (one-way ANOVA followed by Tukey's post hoc test). (e) Representative Hoechst (blue) and DIC images of Control, FLASH- and CONV-irradiated astrocytic cells at 72 h. Cell death was assessed by nuclear condensation and fragmentation. Three subfields per well (100 - 150 cells each), n = 9 wells/condition from 3 independent cultures. Scale bar: 20 µm. (f) qRT-PCR analysis of senescence markers *p53, p21* and *p16* at indicated time points after irradiation. Data are mean ± SEM (n = 3 independent experiments). *p < 0.05 *vs* Control; #p < 0.05 FLASH *vs* CONV (one-way ANOVA followed by Tukey's post hoc test).

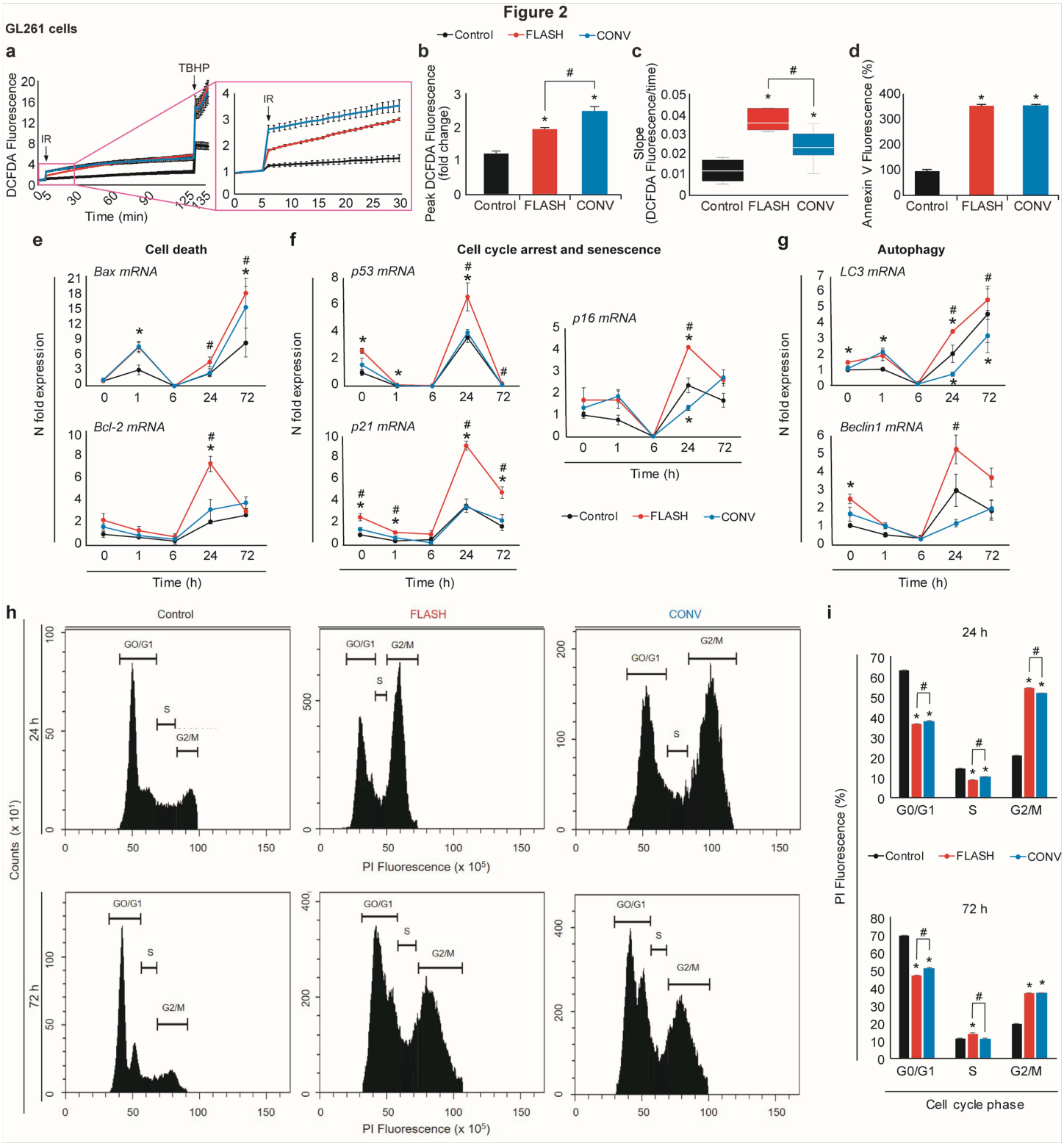


Figure 2

FLASH-RT induces prolonged ROS accumulation and transcriptional activation of stress- and autophagy-related pathways in GL261 cells, accompanied by G2/M accumulation (a - c) Real-time ROS analysis after 8 Gy FLASH- or CONV-RT. FLASH induced a lower early ROS peak (b) but a higher rate of ROS accumulation over time (c). Data are mean ± SEM (n = 3 independent experiments). *p < 0.05 *vs* Control; #p < 0.05 FLASH *vs*CONV (one-way ANOVA followed by Tukey's post hoc test). (d) Flow

cytometry analysis of Annexin V staining, expressed as percentage of Annexin V-fluorescence relative to control, 72 h after 8 Gy FLASH- or CONV-RT. Data are mean ± SEM (n = 3 independent experiments). *p < 0.05 *vs* Control; #p < 0.05 FLASH *vs* CONV (two-way ANOVA followed by Tukey's post hoc test). (e - g) qRT-PCR analysis of genes involved in apoptosis (*Bax, Bcl-2*), senescence (*p53, p21, p16*), and autophagy (*LC3, Beclin1*) at 0 - 72 h after 8 Gy irradiation. FLASH induced earlier and stronger transcriptional activation of stress-response pathways compared with CONV. Data are mean ± SEM (n = 3independent experiments). *p < 0.05 *vs*Control; #p < 0.05 FLASH *vs* CONV (two-way ANOVA followed by Tukey's post hoc test). (h - i) Cell cycle analysis by PI staining using flow cytometry. Data are expressed as the percentage of PI fluorescence in each phase of the cell cycle, 24 h and 72 h after 8 Gy FLASH- or CONV-RT. Data are mean ± SEM (n = 3 independent experiments). *p < 0.05 *vs*Control; #p < 0.05 FLASH *vs* CONV (two-way ANOVA followed by Tukey's post hoc test).

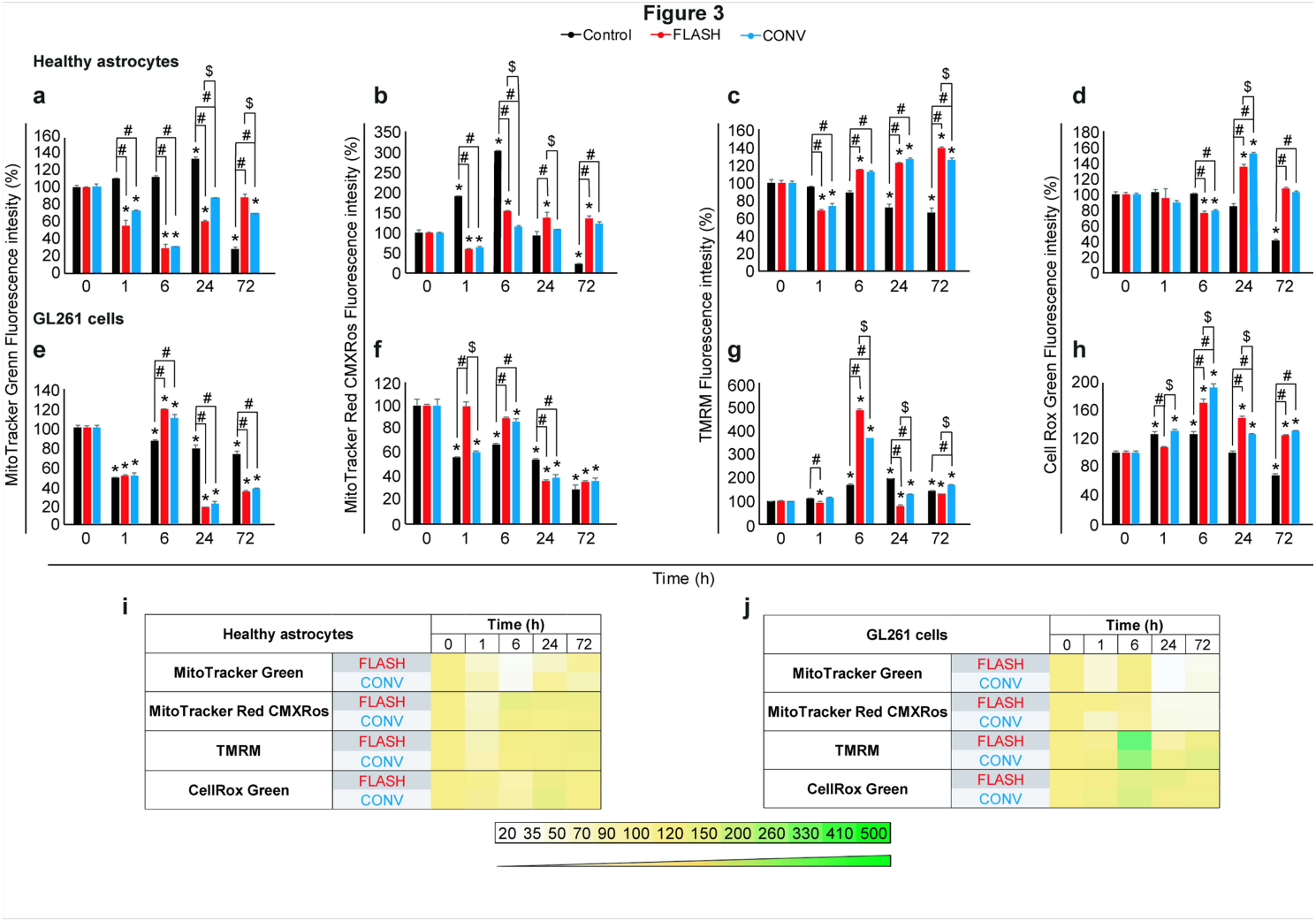


Figure 3

FLASH irradiation preserves mitochondrial function in healthy astrocytes while inducing mitochondrial dysfunction and ROS accumulation in GL261 cells (a - h) Flow cytometry analysis of mitochondrial mass (MitoTracker Green; a, e), active mitochondria (MitoTracker Red CMXROS; b, f), mitochondrial membrane potential (TMRM; c, g), and intracellular ROS (CellROX; d, h) in healthy astrocytes and GL261 cells at 0 -

72 h after 8 Gy FLASH- or CONV-RT. Data are normalized to baseline control. Data are mean ± SEM (n = 3 independent experiments). *p < 0.05 *vs* baseline (0); #p < 0.05 between conditions; $p < 0.05 FLASH *vs*CONV(two-way ANOVA followed by Tukey's post hoc test). Heat maps summarize the flow cytometry-based measurements in healthy astrocytes and GL261 glioma cells following FLASH- or CONV-RT, highlighting the temporal evolution of mitochondrial and oxidative stress responses. Color intensity represents relative normalized signal intensity, with increasing values indicated by a yellow-to-green color gradient.

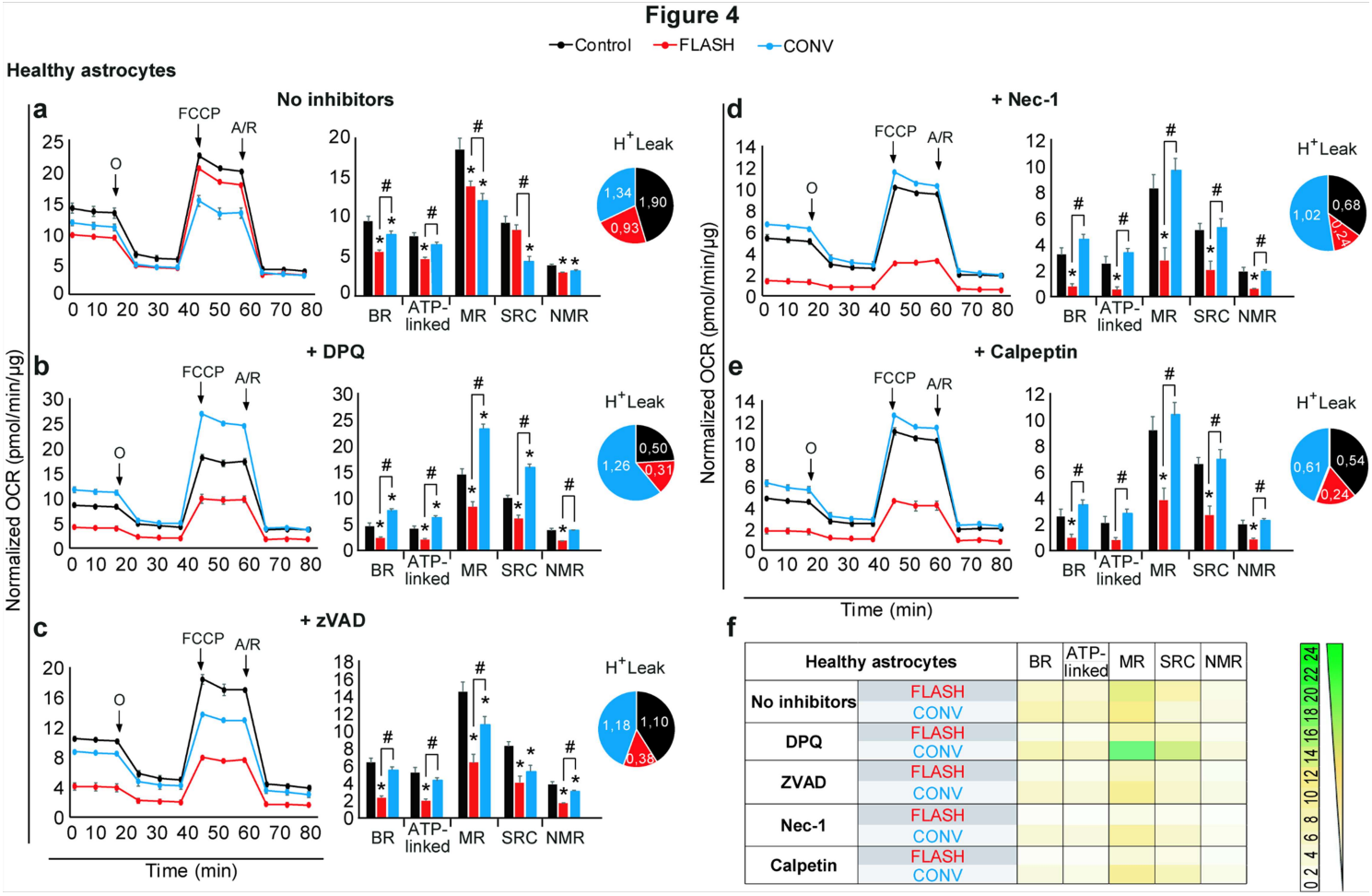


Figure 4

FLASH-RT preserves mitochondrial bioenergetic flexibility in healthy astrocytes with limited contribution of regulated cell death pathways Seahorse XF extracellular flux analysis of mitochondrial respiration in healthy astrocytes (a -e) following FLASH- or CONV-RT, performed in the absence or presence of pharmacological inhibitors (DPQ, zVAD, Nec-1, and Calpeptin) targeting distinct cell death pathways. Mitochondrial bioenergetic parameters include basal respiration (BR), ATP-linked respiration, maximal respiration (MR), spare respiratory capacity (SRC), non-mitochondrial respiration (NMR), and proton leak. Data are presented as mean ± SEM (n = 3 - 4 independent experiments). *p < 0.05 *vs* Control; #p < 0.05 FLASH *vs* CONV (one-way ANOVA followed by Tukey's post hoc test). Heat maps summarize the Seahorse extracellular flux measurements obtained in healthy astrocytes after FLASH- or CONV-RT,

in the absence or presence of pharmacological inhibitors. Color intensity represents relative normalized metabolic activity, with increasing values indicated by a yellow-to-green gradient, highlighting metabolic differences between irradiation modalities and pathway inhibition conditions.

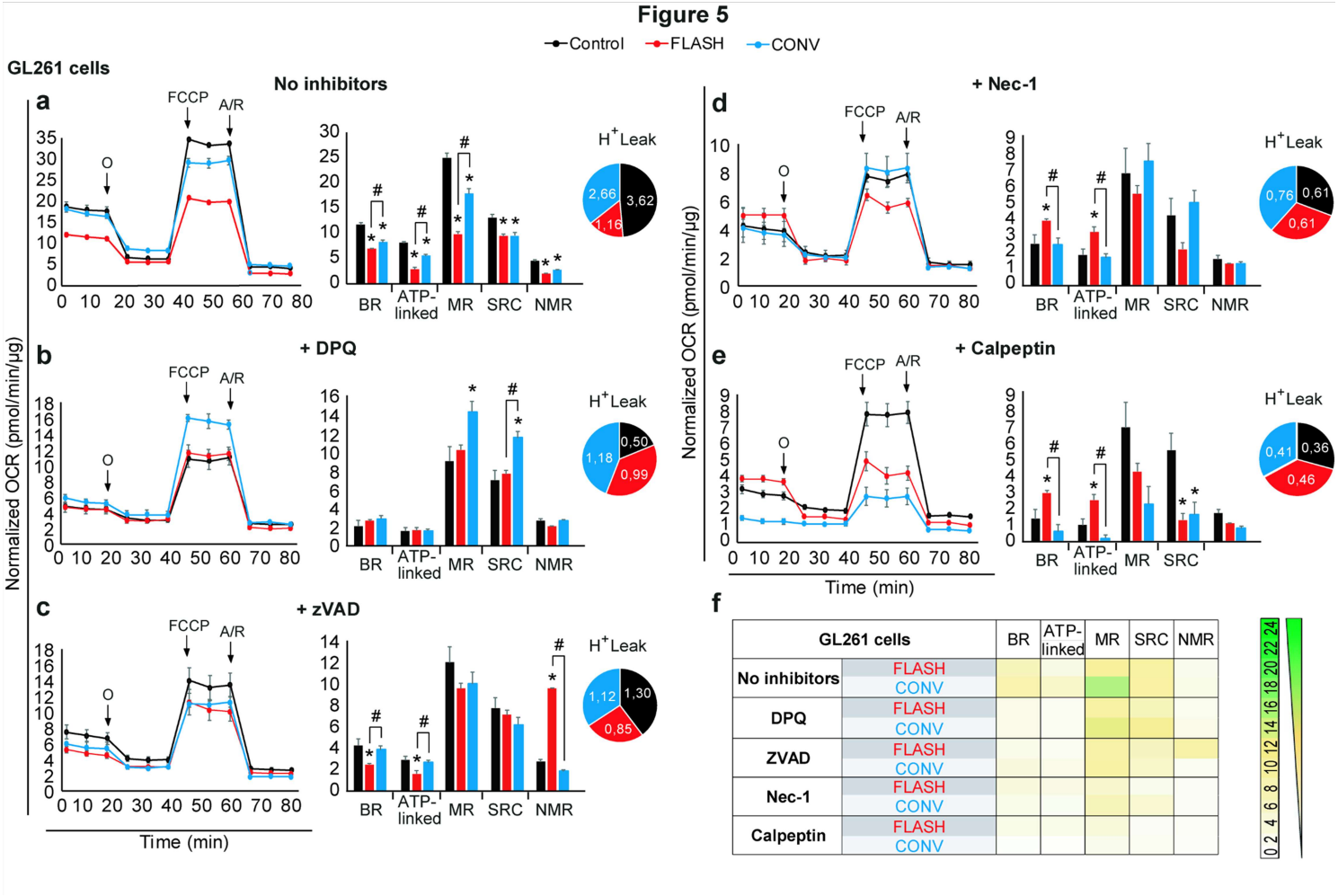


Figure 5

FLASH-RT induces persistent mitochondrial respiratory suppression in GL261 glioma cells with contributions from multiple regulated cell death pathways Seahorse XF extracellular flux analysis of mitochondrial respiration in GL261 cells (a - f) following FLASH- or CONV-RT, performed in the absence or presence of pharmacological inhibitors (DPQ, zVAD, Nec-1, and Calpeptin) targeting distinct cell death pathways. Data are presented as mean ± SEM (n = 3 - 4 independent experiments). *p < 0.05 *vs* Control; #p < 0.05 FLASH *vs* CONV (one-way ANOVA followed by Tukey's post hoc test). Heat maps summarize the Seahorse extracellular flux measurements obtained in GL261 cells after FLASH- or CONV-RT, in the absence or presence of pharmacological inhibitors. Color intensity represents relative normalized metabolic activity, with increasing values indicated by a yellow-to-green gradient, highlighting differences in mitochondrial metabolism between irradiation modalities and pathway inhibition conditions.

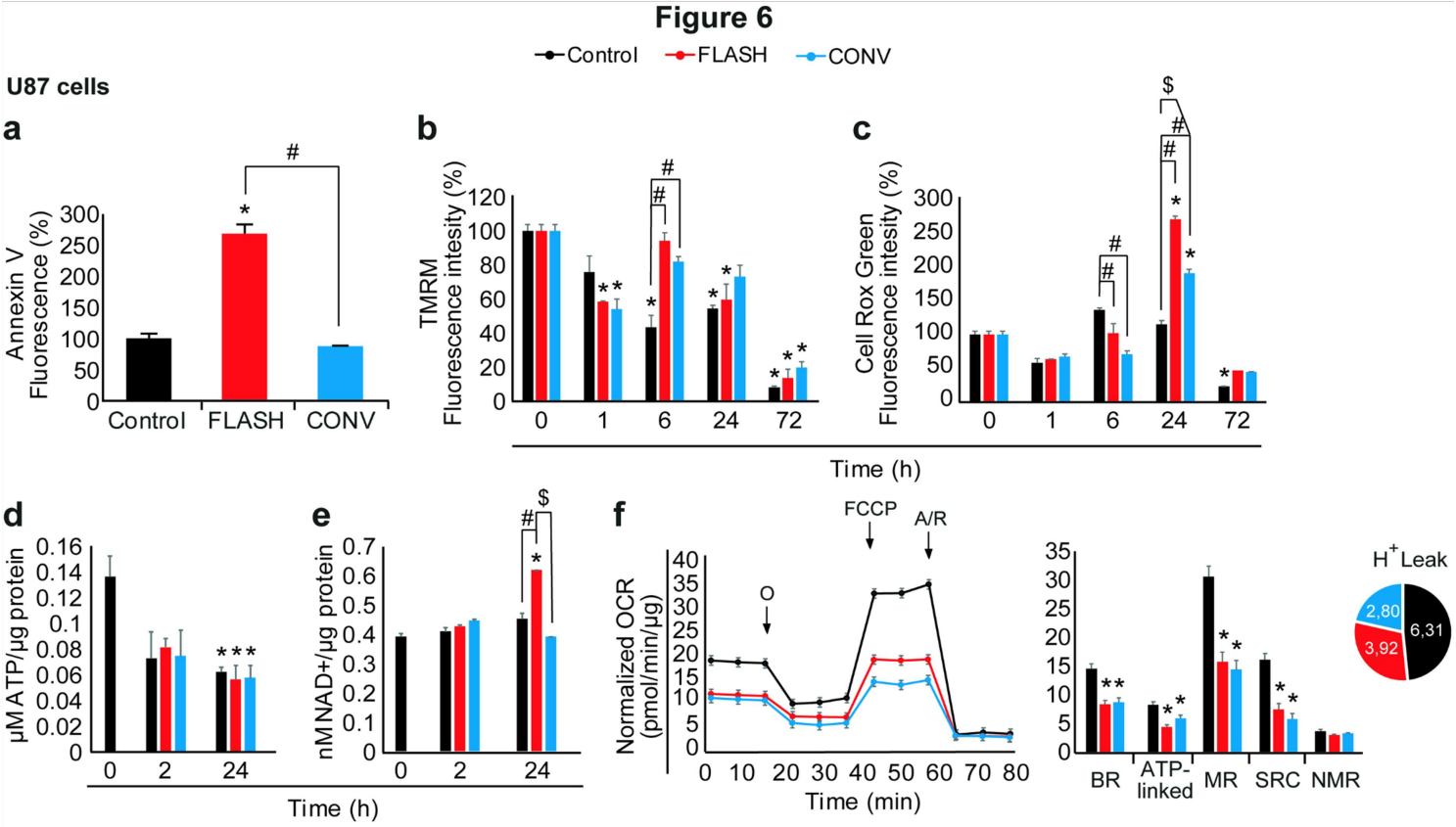


Figure 6

FLASH-RT enhances oxidative stress and impairs mitochondrial bioenergetics in human U87 glioma cells (a) Flow cytometry analysis of Annexin V staining in U87 cells, expressed as percentage of Annexin V fluorescence relative to control, 72 h after 8 Gy FLASH- or CONV-RT. Data are mean ± SEM (n = 3 independent experiments). *p < 0.05 *vs* Control; #p < 0.05 FLASH *vs* CONV (one-way ANOVA followed by Tukey's post hoc test).(b, c) Flow cytometry analysis of mitochondrial membrane potential (TMRM; b) and intracellular ROS (CellROX; c) in U87 glioblastoma cells at 0 - 72 h after 8 Gy FLASH- or CONV-RT. Data are normalized to baseline Control. Data are mean ± SEM (n = 3 independent experiments). *p < 0.05 *vs* baseline (0); #p < 0.05 between conditions; $p < 0.05 FLASH *vs* CONV (two-way ANOVA followed by Tukey's post hoc test). (d) Quantification of intracellular ATP levels in U87 cells at 0, 2, 24 h after 8 Gy FLASH- or CONV-RT. Data are normalized to protein content.Data are mean ± SEM (n = 3 independent experiments). *p < 0.05 *vs* baseline (0); #p < 0.05 *vs* Control; $p < 0.05 FLASH *vs*CONV(two-way ANOVA followed by Tukey's post hoc test). (e) Quantification of intracellular NAD^+ levels in U87 cells at 0, 2, 24 h after 8 Gy FLASH- or CONV-RT. Data are normalized to protein content. *p < 0.05 *vs* baseline (0); #p < 0.05 *vs* Control; $p < 0.05 FLASH *vs*CONV(two-way ANOVA followed by Tukey's post hoc test). (f) Seahorse XF extracellular flux analysis of mitochondrial respiration in U87 cells following 8 Gy of FLASH- or CONV-RT. Data are presented as mean ± SEM (n = 3 - 4 independent experiments). *p < 0.05 *vs* Control; #p < 0.05 FLASH *vs* CONV (one-way ANOVA followed by Tukey's post hoc test).

Supplementary Files

This is a list of supplementary files associated with this preprint. Click to download.

- Table1.docx
- Table2.docx
- Supplementaryinformationfinal.docx
- FigS1.tif
- FigS2.tif
- FigS3.tif